ORNL
MASTER COPY

OAK RIDGE NATIONAL LABORATORY

operated by

UNION CARBIDE CORPORATION

for the

U.S. ATOMIC ENERGY COMMISSION

ORNL-TM-34

CHEMICAL TECHNOLOGY DIVISION

UNIT OPERATIONS SECTION

MONTHLY PROGRESS REPORT

JUNE 1961

NOTICE

This document contains information of a preliminary nature and was prepared primarily for internal use at the Oak Ridge National Laboratory. It is subject to revision or correction and therefore does not represent a final report. The information is not to be abstracted, reprinted or otherwise given public dissemination without the approval of the ORNL patent branch, Legal and Information Control Department.

LEGAL NOTICE

This report was prepared as an account of Government sponsored work. Neither the United States, nor the Commission, nor any person acting on behalf of the Commission:

A. Makes any warranty or representation, expressed or implied, with respect to the accuracy, completeness, or usefulness of the information contained in this report, or that the use of any information, apparatus, method, or process disclosed in this report may not infringe privately owned rights; or

B. Assumes any liabilities with respect to the use of, or for damages resulting from the use of any information, apparatus, method, or process disclosed in this report.

As used in the above, "person acting on behalf of the Commission" includes any employee or contractor of the Commission, or employee of such contractor, to the extent that such employee or contractor of the Commission, or employee of such contractor prepares, disseminates, or provides access to, any information pursuant to his employment or contract with the Commission, or his employment with such contractor.

ORNL-TM-34

UNIT OPERATIONS SECTION MONTHLY PROGRESS REPORT

June 1961

CHEMICAL TECHNOLOGY DIVISION

M. E. Whatley

P. A. Haas
R. W. Horton
A. D. Ryon
J. C. Suddath
C. D. Watson

Date Issued

JAN 23 1962

OAK RIDGE NATIONAL LABORATORY
Oak Ridge, Tennessee
Operated By
UNION CARBIDE CORPORATION
for the
U. S. Atomic Energy Commission

ABSTRACT

An interfacial viscosimeter has been built for use in an interfacial phenomena study. Installation of a 6-in.-ID foam separation column system was completed. The dispersion-drying-sintering characteristics of six low-nitrate batches of thoria sol material were studied. The average effective porosity of the CuO pellets used for reactor helium purification was determined to be 0.0545 for H_2 transport and 0.0526 for CO transport. In continuous Zirflex dissolution studies no H_2O_2 decomposition was observed when 10% H_2O_2 was fed into boiling dissolvent through a water-cooled nozzle and the oxygen concentration in the scrubbed off-gas could be used to control the H_2O_2 concentration in the dissolver. The free fluoride in Zirflex solutions must be maintained above 1 molar in order to prevent uranium precipitation at low concentrations of uranium even though the F^-/U ratio exceeds 100. Chopped stainless steel clad UO_2 sections were leached in a 4 stage pyrex leacher model using 6, 7, and 8 M nitric acid as the dissolvent. The temperature distribution expected within fuel elements consisting of square arrays of tubes has been calculated for shipping conditions assuming heat be transferred only by radiation. HETS values were calculated for uranium stripping under 5% TBP flowsheet conditions. Very fine particles were obtained by quenching fused salt droplets in water. A waste calcination run was made using TBP-25 waste and the close coupled evaporator calciner system.

CONTENTS

		Page
	Abstract	2
	Previous Reports in This Series	4
	Summary	5
1.0	Chemical Engineering Research	8
2.0	Fuel Cycle Development	14
3.0	GCR Coolant Purification Studies	17
4.0	Power Reactor Fuel Processing	23
5.0	Reactor Evaluation Studies	32
6.0	Solvent Extraction Studies	39
7.0	Volatility	44
8.0	Waste Processing	56

PREVIOUS REPORTS IN THIS SERIES

CF Numbers for UNOP Monthly Reports

December	1954 (Part I-HR)	55-1-45
December	1954 (Part II)	55-1-62
January	1955	55-1-194
February	1955	55-2-185
March	1955	55-3-190
April	1955	55-4-164
May	1955	55-5-179
June	1955	55-6-180
July	1955	55-7-138
August	1955	55-8-157
September	1955	55-9-150
October	1955	55-10-110
November	1955	55-11-176
December	1955	55-12-154
January	1956	56-1-175
February	1956	56-2-154
March	1956	56-3-177
April	1956	56-4-210
May	1956	56-5-197
June	1956	56-6-177
July	1956	56-7-150
August	1956	56-8-215
September	1956	56-9-127
October	1956	56-10-83
November	1956	56-11-143
December	1956	56-12-128
January	1958	58-1-137
February	1958	58-2-139
March	1958	58-3-71
April	1958	58-4-123
May	1958	58-5-50
June	1958	58-6-85
July	1958	58-7-126
August	1958	58-8-59
September	1958	58-9-62
October	1958	58-10-90
November	1958	58-11-93
December	1958	58-12-35
January	1959	59-1-74
February	1959	59-2-45
March	1959	59-3-61
April	1959	59-4-47
May	1959	59-5-47
June	1959	56-6-63
July	1959	59-7-58
August	1959	59-8-76
September	1959	59-9-69
October	1959	59-10-77
November	1959	59-11-54
December	1959	59-12-49

Chemical Technology Division Monthly Reports

January	1957	ORNL-2251
February	1957	ORNL-2270
March	1957	ORNL-2307
April	1957	ORNL-2324
May	1957	ORNL-2361
June	1957	ORNL-2362
July	1957	ORNL-2385
August	1957	ORNL-2400
September	1957	ORNL-2416
October	1957	ORNL-2417
November	1957	ORNL-2447
December	1957	ORNL-2468
January	1960	60-1-49
February	1960	60-2-56
March	1960	60-3-61
April	1960	60-4-37
May	1960	60-5-58
June	1960	60-6-11
July	1960	60-7-46
August	1960	60-8-86
September	1960	60-9-43
October	1960	60-10-49
November	1960	60-11-38
December	1960	60-12-28
January	1961	61-1-27
February	1961	61-2-65
March	1961	61-3-67
April	1961	ORNL-TM-32
May	1961	ORNL-TM-33
June	1961	ORNL-TM-34

SUMMARY

1.0 CHEMICAL ENGINEERING RESEARCH

1.1 Interfacial Phenomena in Mass Transfer

An interfacial viscosimeter has been built for use in an interfacial phenomena study. In a preliminary experiment, the viscosity of the air-water interface of a solution containing 10 ppm of the commercial detergent "Tide" was measured as 0.95 two-dimensional centipoise at 25°C. The sensitivity of the instrument appears to be on the order of 10^{-4} two-dimensional poise (i.e., dyne-sec/cm).

1.2 Foam Separation

Installation of a 6-in.-ID foam separation column system was completed. The 0.4-in.-dia cyclone used as a foam breaker gave a wet foam about 1/500th of the inlet foam volume. An altered column top was required to eliminate liquid level surging induced by the cyclone foam breaker. An altered feed distributor reduced, but did not eliminate, channeling in the column.

2.0 FUEL CYCLE DEVELOPMENT

The dispersion-drying-sintering characteristics of six representative low-nitrate batches (N/Th ratios from 0.040 to 0.066) were studied. A minimum dispersion of 98 wt % was obtained for all these powders at N/Th ratios of ~0.11. Portions of these same batches, which were leached in hot water (80°C) and dried immediately after denitration, required N/Th ratios between 0.15 and 0.19 for dispersion. Toluene densities for all sintered products ranged from 9.76 to 9.88 g/cc and were apparently independent of the N/Th ratio. Eight fuel pins containing ThO_2-UO_2 prepared in the laboratory by this process and vibratorily compacted to 8.6 or 8.7 g/cc have performed satisfactorily for the initial two months of irradiation in the NRX reactor. These 5/16-in.-OD elements loaded with 4.3 wt % enriched UO_2 will probably accumulate 8,000 to 15,000 megawatt days/metric ton of Th at 300,000 Btu/hr-ft^2 surface heat flux.

3.0 GCR COOLANT PURIFICATION STUDIES

The average effective porosity of CuO pellets was determined to be 0.0545 for H_2 transport and 0.0526 for CO transport based on the reaction of H_2 or CO with CuO pellets in differential bed tests. The expression for the mass transfer factor of H_2 across an external gas-film surrounding a CuO pellet as a function of Reynold's Number was determined to be, $J_D = 0.24\ (Re')^{-0.69}$.

4.0 POWER REACTOR FUEL PROCESSING

4.1 Modified Zirflex

In continuing studies of the dissolution of U-Zr-Sn in NH_4F-NH_4NO_3-H_2O_2 no gassing (indicating H_2O_2 decomposition in the line) was observed when 10%

H_2O_2 was fed into boiling dissolvent through a water-cooled nozzle. The behavior of the O_2 concentration in the scrubbed off-gas with time indicated that the continuous H_2O_2 addition rate could be controlled by maintaining ~3 ± 2% O_2 in the off-gas (principally hydrogen). The presence of as much as 1% O_2 has indicated a sufficient H_2O_2 addition to maintain U^{VI} in the dissolvent. While a reasonable excess of H_2O_2 is not harmful in the dissolution, limiting the off-gas O_2 concentration to $\leq$ 5% avoids the flammable range for O_2-H_2 mixtures (lower limit for O_2 in hydrogen is 6%).

In engineering-scale runs dissolving 8% U-ZrH a small amount (< 1% of fuel charged) of a green precipitate containing 60% U, 23% F, and 6.4% Zr formed when the final free F^-/U ratio $\leq$ 82. A similar amount of precipitate formed at F^-/U = 115 when dissolving 2% U-Zr-Sn (PWR seed). Here a higher F^-/U ratio resulted from a much lower free F^- concentration since the U was lower by a factor of 4. This indicated that not only must a free F^-/U ratio of 90-100 be maintained (controlling for high U fuels) but also the free F^- M of the dissolvent must not drop below ~1 M (limiting for low U fuels) if total dissolution without precipitation is to be accomplished.

4.2 Shearing and Leaching

The composite product when leaching the UO_2 from chopped stainless steel clad UO_2 sections, 1/2-in.-OD x 1-in. long, in the 4 stage pyrex leacher model using 6, 7, and 8 M HNO_3 as the dissolvent was 325 g U/liter and 2.5 M HNO_3, 350 g U/liter and 3.0 M HNO_3, and 425 g U/liter and 3.0 M HNO_3.

5.0 REACTOR EVALUATION STUDIES

5.1 Heat Transfer from Spent Fuel Elements during Shipping

The temperature distributions expected within fuel elements during shipping if heat could be transferred only by radiation have been calculated. These results are reasonably close to the temperatures obtained from experimental measurements with electrically heated mock fuel elements and a simulated shipping carrier, especially at higher heat generation rates. Calculations for a 36 tube bundle and a heat generation rate of 0.0986 watts/cm had an average deviation from the measured temperatures of approximately 16°C, and the maximum temperature could generally be predicted more closely than this. However, there were still noticeable effects of convection such as non-uniform carrier wall temperatures and unsymmetrical temperatures about the horizontal plane through the center of the bundle.

6.0 SOLVENT EXTRACTION STUDIES

HETS values were calculated for uranium stripping under 5% TBP flowsheet conditions. HETS values were ~2.0 feet for aqueous continuous operation of the sieve plate column and for solvent continuous operation of the nozzle plate column regardless of the pulse frequency used. An aqueous continuous operation of the nozzle plate column resulted in a HETS value of 3.1 feet for the pulse frequencies tested.

7.0 VOLATILITY

Fused NaF, LiF, ZrF_4 salt was sprayed with two fluid atomizing nozzles for 15 min obtaining a mean droplet size of ~60 micron. Very fine particles (< 5 micron) were obtained by water quenching the hot droplets.

8.0 WASTE PROCESSING

Using simulated TBP-25 waste, the evaporator-calciner close coupled system was operated under continuous control conditions. Control of the system was satisfactory during the complete test, except for one time period (one hour duration) when the evaporator was upset by foaming and a plugged liquid level probe. Stable ruthenium was added to the feed to follow its behavior during the test. By chemical analysis the only ruthenium in the system at the end of the test was in the calciner and the liquid heel of the evaporator. The ruthenium in the evaporator condensate was below the detectable concentration. Mercury behaved similar to the ruthenium except its concentration increased in the evaporator heel during the calcination period.

1.0 CHEMICAL ENGINEERING RESEARCH

1.1 Interfacial Phenomena in Mass Transfer - C. V. Chester

Previous studies on the water-uranyl nitrate-tributyl phosphate system indicate that in solvent extraction contactors the rate-limiting process for the extraction of uranyl nitrate is diffusive and convective transport of the molecular species concerned to and from the interface. Many investigators have found that certain interfacial phenomena, such as interfacial turbulence, and interfacial pressure caused by surface active agents, can have a profound effect on the rate of mass transfer in solvent extraction.

To obtain basic information on the mechanics of contactor operation, studies of the hydrodynamics of solvent extraction system interfaces are being undertaken. It is believed that such studies will lead to improved design of contactors and contactor operation. One of the interfacial properties of interest is that of two-dimensional shear viscosity. This plays a role in the reduction of drop circulation and interfacial turbulence, to the detriment of mass transfer. The presence of surface active agents increases interfacial viscosity.

An interfacial viscosimeter has been designed and constructed (Figures 1.1 and 1.2). It is essentially a modified two-dimensional Brookfield viscosimeter. A stationary ring is suspended in the interface by a fine wire of known torsional spring constant. A ring surrounding the stationary ring with a known clearance is rotated at constant velocity. From the torque produced in the stationary ring by the shear in the interface, the interfacial viscosity can be calculated. Momentum transfer from the rotating to the stationary ring is minimized by appropriate baffles, and can be separately measured and compensated for.

Before operation, the instrument had to be carefully adjusted so that all the parts were co-axial. The torsional spring constant of the wire was determined by giving a small angular displacement to the inner ring and then measuring its period of oscillation (45 sec). The period is equal to the square root of the ratio of the moment of inertia of the ring (223.4 g cm^2) to the spring constant of the wire. The spring constant was 0.1104 dyne-cm/radian.

In operation, the instrument was leveled up in a crystallizing dish, and the rest position of the inner ring noted. The motor was connected to the drive shaft and started. Distilled water was slowly added until the interface was between the rings. The rotation of the drum dial necessary to restore the ring to its rest position (through torsion on the wire) was noted (120°). The water level was then raised until the top surfaces of both rings were submerged, and hence no longer in the interface. The torque on the inner ring was continuously increasing during this process, and the drum reading was 220° when the rings were finally wet.

Water was pipetted from the system until the level was again below both rings. When the rings had dried, the rest position was again noted (0°). The level was raised again to the interface position between the

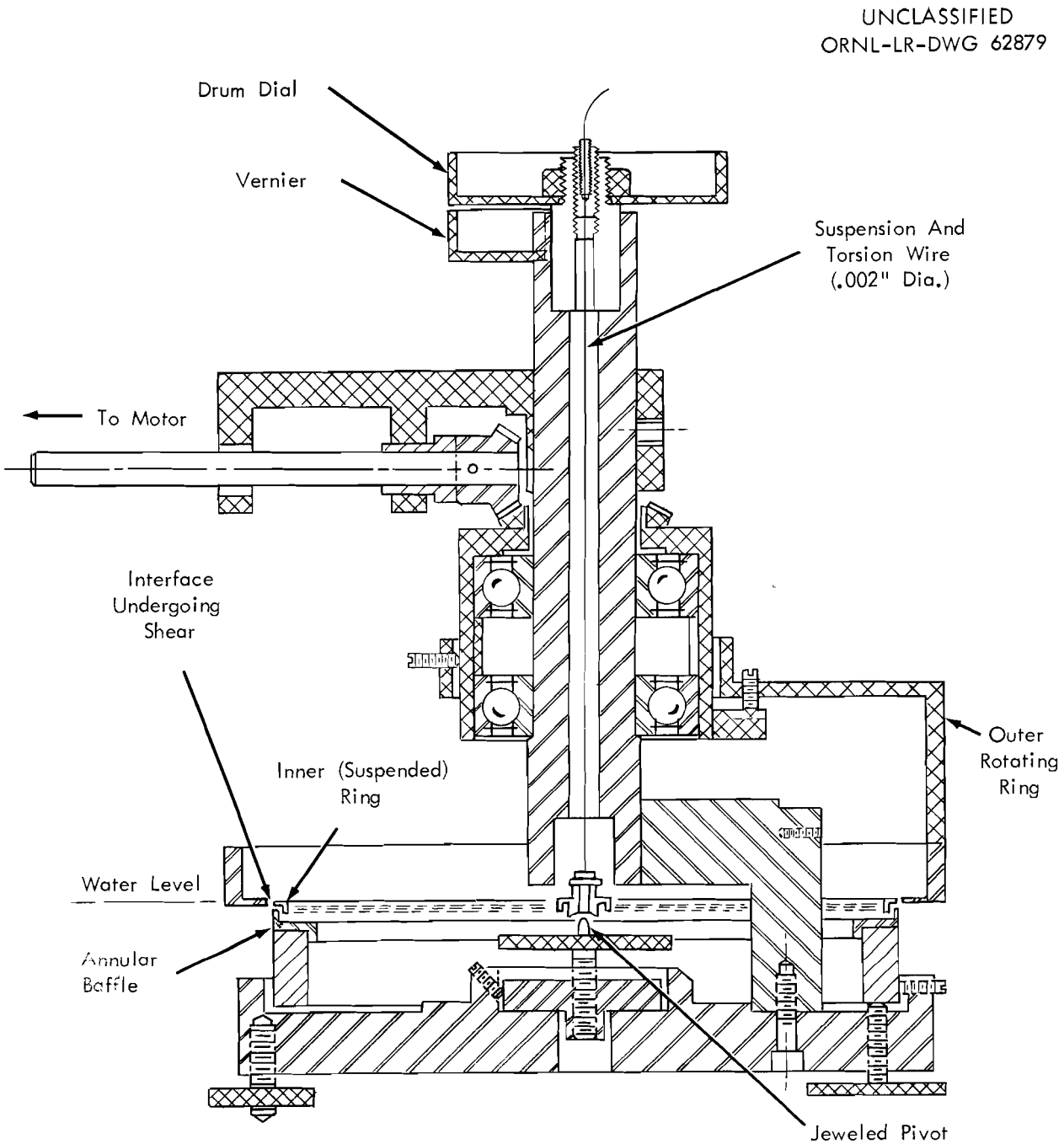

Fig. 1.1. Interfacial viscosimeter (set up for air-water interface).

Fig. 1.2. Interfacial viscosimeter setup.

rings, and the deflection noted (120°). Then 10 ppm of the commercial detergent "Tide" was added to the system. In a few seconds the inner ring began to follow the rotating ring. At equilibrium, four complete turns on the drum dial (1440°) were required to bring the inner ring to its rest position, with the outer ring making 9 revolutions per minute.

When the level of the solution was raised until the surfaces of the rings were just submerged, the drum reading was 220°, the same as without the detergent.

The fact that there was no observed decrease in deflection when the clean interface passed the upper surfaces of the rings indicates that the viscosity of the clean interface per se is below detection in the experiment.

From the radius of the ring (5.59 cm) and the separation of the two rings (0.10 cm) the effective shear viscosity of the interface was calculated as 0.95 two-dimensional centipoise in a shear field of 52.7 cm/sec, cm. The shear field is specified as it is expected the interface may not be Newtonian, in the two-dimensional sense. The viscosity measured is in the range found by Harkins ("Physical Chemistry of Surface Films," Reinhold, 1952) for monolayers of fatty acids on water.

In the immediate future, some of the reported surface viscosities will be checked quantitatively, and then some interfacial (liquid-liquid) viscosities will be measured.

1.2 Foam Separation - P. A. Haas, W. W. Wall, Jr.

Engineering studies of foam-liquid contacting columns as separation systems have started at ORNL. An application of immediate interest would be the removal of certain fission products from waste. Studies of the chemistry of foam and surface active agents in Chemical Development Section B have determined systems of interest for waste processing. A 6-in.-ID foam column system (Figure 1.3) was installed in Cell 3 of Bldg. 4505. Calibration of flowmeters and preliminary checkout operation of the system were completed.

The 0.40-in.-dia cyclone condensed the foam to a liquid and a small volume of wet foam. During one two-hour test period, the liquid and wet foam volume was 1/500th of the column foam volume. Effective condensation was not obtained when the flow was reduced to the 3 liter/min column foam rate. The usual operating conditions were atmospheric pressure at the top of the column and cyclone discharge to house vacuum. Flow rate-condensation efficiency-pressure drop measurements remain to be determined. Cyclic pressure variations of several inches of water, several cycles per minute in the column were observed when the column vent was a 3/8-in. tubing tee in the column to cyclone line. Substitution of a 2-in.-ID tee at the column top as a vent eliminated these fluctuations and results in excellent liquid level control by use of the jackleg.

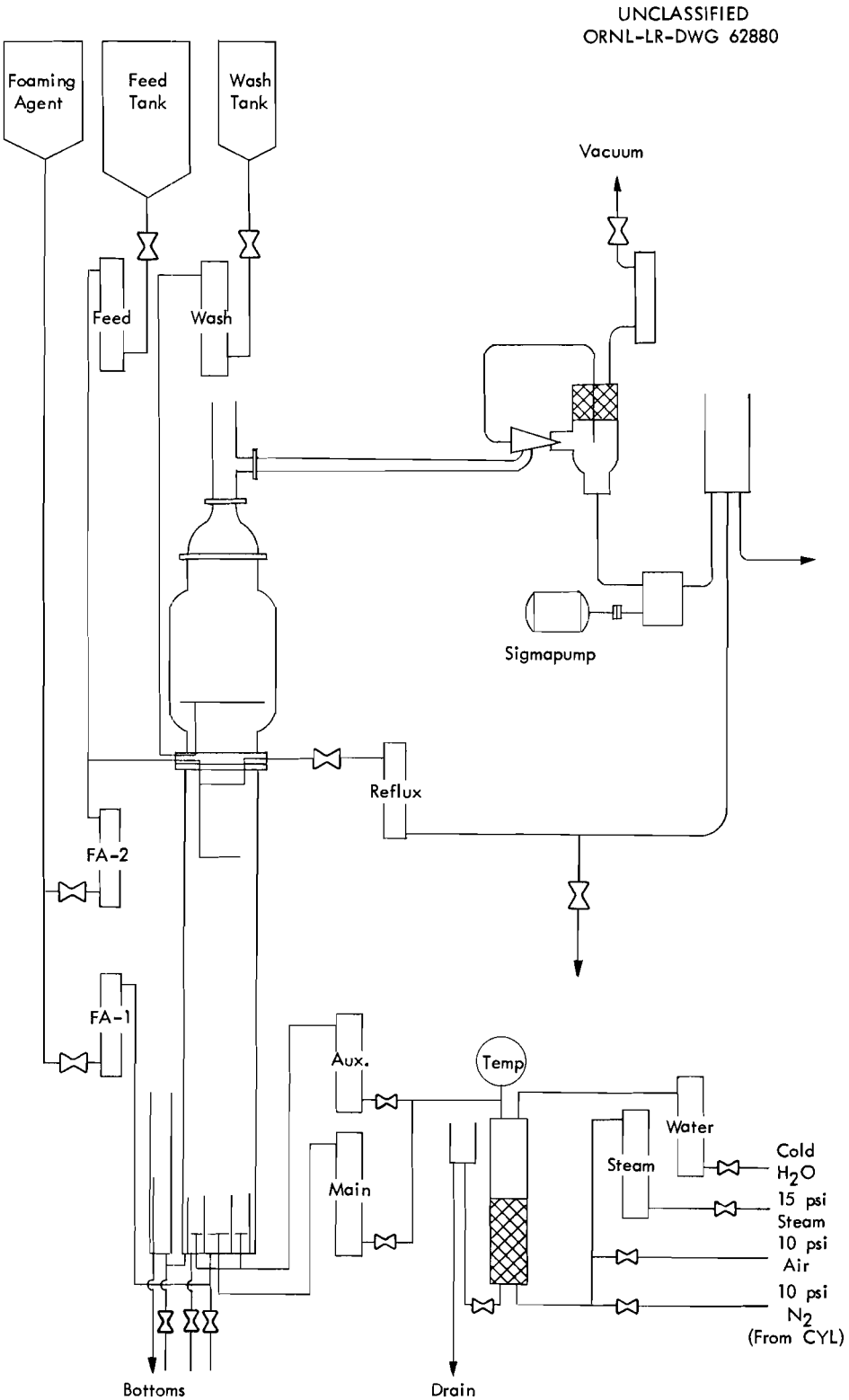

Fig. 1.3. Foam separation column system.

Channeling of liquid in the 6-in.-dia column was evident from regions of foam downflow at velocities up to 3 cm/sec when the net foam flow was 0.1 to 0.4 cm/sec upward. The amount of channeling was reduced when the distribution of the liquid feed across the column cross section was improved. The amount of channeling varied with foam and liquid flow rates, but some channeling was observed for all combinations of 1000 to 4000 cc/min foam rates and 100 to 1300 cc/min liquid feed rates.

2.0 FUEL CYCLE DEVELOPMENT

P. A. Haas

The fuel cycle program is a study of fuel materials preparation and fuel element fabrication procedures economically adaptable to remote operation for recycle of fissile and fertile materials. Vibratory compaction of high density ThO_2 or ThO_2-UO_2 particles has been selected as a promising method for remote loading of cladding tubes. Denitration of $Th(NO_3)_4$ in steam atmospheres gives products which can be converted into thoria or thoria-urania sols and then dried and calcined into oxide particles of near theoretical density. The present emphasis is on engineering development of these oxide preparation steps and on the irradiation of test elements of vibratorily compacted oxides.

2.1 Oxide Preparation Development - C. C. Haws, Jr., J. W. Snider, R. D. Arthur

Six runs were made in the trough calciner to determine the reproducibility of the operation and to furnish a number of representative low-nitrate feed materials for drying-dispersion-sintering studies. The N/Th ratio was held between 0.048 and 0.066 (Table 2.1). By adding nitric acid to a total N/Th ratio of ~0.11, all batches were dispersed to $\geqq$ 98 wt %. These dispersions have the lowest nitrate content of any thoria sols made to date and offer an opportunity to study the properties of materials produced from low nitrate thorias.

No discernible relationships were found between sintered product density, screen size analysis and the N/Th ratio of the sols. Sintered thoria from these samples averaged above 9.8 g/cc density, while previous sinters from higher ratio denitrator products (N/Th = 0.15 - 0.20) averaged above 9.7 g/cc. This could mean that density of the sintered sample is more dependent upon the nitrogen content of the original powder than it is upon the immediate concentration of the sol from which it is prepared. All samples yielded more than 90 wt % of the coarse +16 mesh shards, easily adequate to meet the requirements of the present vibratory compaction mix of 60 wt % 10/16 mesh material. For reference, a 1500 g sample of thoria (screen 75 wt % +16 mesh material) yielded 64 wt % of +16 mesh shards when ground and screened for vibratory compaction.

It was assumed in the past that a water leaching (80°C for 1 hr with constant agitation) would leach out or disperse the "high nitrate" thoria, leaving behind "low nitrate" thoria in the "insolable" heel. This supposition had never been thoroughly checked. The results of these tests do not bear out this assumption; the thoria in the sedimentary layer is approximately as rich in nitrogen as is the supernatant layer within the uncertainty of results (Table 2.1). Also the quantity of material dispersible in hot water increased with time following denitration. For example, Sample No. 18U dispersed only 0.75 wt % in hot water immediately after denitration, but a duplicate sample dispersed 5.6% after storage for about three weeks. This aging phenomenon does not occur in the "insolable" heel left after extraction with water (the "T" samples). The "U" designates the original, untreated

Table 2.1. Characteristics of Sol Gel Process Products Prepared from Low Nitrate Thoria Sols

Dispersion Conditions: One hour with agitation at 80°C, 2 M Th

Run No.	Feed[a] Material N/Th Ratio	Wt % Dispersion in Water Only: Immediately After Denitration	Wt % Dispersion in Water Only: Three Weeks After Denitration	Nitric Acid-Water Dispersions[b]: Wt % Dispersed	Nitric Acid-Water Dispersions[b]: Sol N/Th Ratio	Sintered Product Density g/cc	Screen Size Analysis (weight %): +16	Screen Size Analysis (weight %): 16/100	Screen Size Analysis (weight %): -100
18U	0.0502	0.75	5.6	-	0.107	9.76	92.5	7.2	0.3
18T	0.0484		0		0.163	9.77	94.6	5.1	0.3
19U	0.0661	1.6	33.2	99.7	0.109	9.85	97.1	2.8	0.1
19T	0.0592		5.2		0.159	9.88	95.7	3.9	0.4
20U	0.0517	4.1	1.6	99.4	0.109	9.85	94.8	4.9	0.3
20T	0.0462		0		0.146	9.78	92.9	6.5	0.6
21U	0.0517	0.66	3.2	98.6	0.109	9.87	-	-	-
21T	0.0422		0.4		0.118	9.85	95.2	4.4	0.4
22U	0.0559	1.7	6.0	99.8	0.113	9.85	93.3	6.1	0.6
22T	-		0.8		0.194	9.85	92.2	7.8	0
23U	0.0597	0.9	4.0	99.7	0.117	9.83	95.6	4.1	0.3
23T			0.8		0.191	9.84	95.0	4.6	0.4

[a]Estimated mean deviation for "U" samples was 0.005.

[b]Amounts of nitric acid used were minimum amounts which appeared to give complete dispersion.

denitrator product. The dried solid material obtained from the immediate hot water dispersion tests following denitration are given the "T" designation.

2.2 Irradiation Testing - S. D. Clinton, work in cooperation with E. S. Bomar, Metallurgy Division

Eight fuel pins containing ThO_2-UO_2 prepared by Chemical Development Section A have performed satisfactorily in the NRX reactor during the two-month period of April and May. Each specimen contains approximately 75 g of fuel with a fully-enriched uranium content of 4.2 to 4.4 wt %. The fuel, consisting of three different particle size fractions, was loaded into 11 in. long tubes (5/16-in.-OD, 304 SS, 25 mil wall) to bulk densities between 8.6 and 8.7 g/cc by pneumatic vibratory compaction. Five of the tubes were loaded with sol-gel ThO_2-UO_2 prepared from thorium oxalate precipitated thoria, and three tubes were filled with sol-gel ThO_2-UO_2 prepared by steam stripping thorium nitrate.

The eight fuel pins are located in a single channel of a PRFR irradiation holder at the Chalk River NRX reactor. Assuming a cosine flux distribution along the channel length, the unperturbed thermal neutron flux varies between 3.0 and 5.5 x 10^{13} n/cm^2-sec. Using the flux perturbation method of Lewis (Nucleonics, October 1955), the thermal flux is decreased by ~25% within the fuel pins. At a peak perturbed flux of 4 x 10^{13} n/cm^2-sec, the heat flux at the clad surface is 300,000 Btu/hr-ft^2. Due to the uncertainty in the thermal conductivity of the compacted ThO_2-UO_2 particles, the center-line fuel temperature cannot be determined to any degree of accuracy. If an effective k of 1.0 Btu/hr-ft-°F is assumed for the oxide fuel, then the center temperature should not exceed 2250°F. The peak integral of k $d\theta$ for the fuel pins is 18.8 watts/cm which is well below the limits for center melting (50 watts/cm) and increased fission gas release (30 watts/cm) in UO_2 pellets. If the in-pile experiment continues to operate satisfactorily, the fuel specimen should remain in the reactor until burnups in the order of 8,000 to 15,000 megawatt days/metric ton of Th are achieved, depending on the pin location (approximately 230 full power days). The major objectives of the proposed post-irradiation examination are as follows: pressure build-up and chemical analyses of the fission product gases released from the fuel, fission product distribution in the fuel as determined by gamma-ray survey, and void formation or other structural changes in the oxide as determined by metallographic techniques.

Four 11-in. and two 22-in. long tubes were loaded by vibratory compaction with Spencer arc-fused ThO_2-UO_2 containing 3.9 wt % fully-enriched uranium. The fuel bulk density in these tubes is 8.6 g/cc. Similar fuel specimens loaded with sol-gel ThO_2-UO_2 should be completed by the middle of June. The 11-in. tubes will be scheduled for insertion in the MTR at an unperturbed flux of 1 x 10^{14} n/cm^2-sec, and the longer tubes will be placed in the NRX reactor by August of this year. One of the major objectives of those proposed irradiations is to compare the in-pile effects of arc-fused ThO_2-UO_2, which has been formed at temperatures in the order of 3000°C, and sol-gel ThO_2-UO_2, which has been fired to a maximum temperature of 1200°C.

3.0 GCR COOLANT PURIFICATION STUDIES

J. C. Suddath

Contamination of coolant gases by chemical impurities and release of fission products from fuel elements are major problems in gas-cooled reactors and in-pile experimental loops. Investigations are being made to determine the best methods to reduce the impurities, both radioactive and non-radioactive with emphasis on the kinetics of the fixed bed oxidation of hydrogen, carbon monoxide, and methane by copper oxide.

An attempt is being made to fit experimental data from the study of the $CuO-H_2$ and $CuO-CO$ reactions to a mathematical model of external diffusion and internal diffusion of the H_2 or CO controlling a rapid, irreversible reaction.

3.1 Determination of CuO Pellet Effective Porosity - C. D. Scott

With the assumption of external diffusion-internal diffusion controlling the H_2-CuO and CO-CuO reactions it is possible to derive an expression for the effective porosity of the CuO pellet: (see Unit Operations monthly report for March 1961)

$$\alpha = \frac{b}{CtD}\left(\frac{R^2}{6} + \frac{r_o^3}{3R} - \frac{r_o^2}{2}\right) \qquad (1)$$

where

α = effective porosity for H_2 or CO transport within the CuO pellet, effective void volume/total volume

b = molar density of CuO in pellet, g-moles/cc

C = concentration of H_2 or CO in the bulk gas phase, g-moles/cc

t = total time of exposure of pellet to reaction environment, sec

D = molecular diffusivity of H_2 or CO, cm^2/sec

R = radius of CuO pellet, cm

r_o = radius of the Cu-CuO interface in the pellet after reaction, cm

Several differential bed tests were made in which mono-layers of CuO pellets were contacted with a high velocity stream of helium containing constant amounts of H_2 or CO in the temperature range of 400 - 600°C, concentration range of ~0.1 to 1.0 vol % H_2 or CO and at pressures of 10.2, 20.4, and 30 atm (Table 3.1). At the end of each test the position of the Cu-CuO interface (r_o) was measured. This allowed determination of the effective porosity, α, for each set of operating conditions by use of equation (1). If the postulated kinetic mechanism is correct for both the $CuO-H_2$ and CuO-CO reactions, then the determined values of effective porosity should be constant over the range of operating conditions for both H_2 and CO.

Table 3.1. Effective Porosity of CuO Pellets for Molecular Transport of H_2 and CO as Determined from Differential Bed Tests of the H_2-CuO and CO-CuO Reactions

Run No.	Temp., °C	Pressure, atm	Contaminant Concentration, vol %	Number of Cu Pellets	Effective Porosity
			$H_2 + CuO \rightarrow H_2O + Cu$		
1	500	20.4	0.95	7	0.0663
2	400	20.4	0.096	8	0.0550
3	600	20.4	0.65	6	0.0664
4	500	20.4	0.54	11	0.0650
5	400	20.4	0.93	11	0.0476
6	600	20.4	0.46	10	0.0546
7	400	20.4	0.40	11	0.0459
8	500	20.4	0.93	11	0.0441
9	500	20.4	0.091	9	0.0479
10	500	20.4	0.071	9	0.0443
11	400	10.2	0.89	9	0.0674
12	500	10.2	0.65	9	0.0664
13	500	10.2	0.52	9	0.0574
14	600	10.2	1.08	9	0.0596
15	400	10.2	0.82	9	0.0442
16	500	10.2	1.05	9	0.0563
17	400	30.0	0.56	9	0.0449
18	500	30.0	0.51	9	0.0536
19	600	30.0	0.39	9	0.0494
				Average	0.0545
			$CO + CuO \rightarrow CO_2 + Cu$		
1	400	20.4	1.08	12	0.0487
2	500	20.4	1.04	9	0.0475
3	600	20.4	1.02	9	0.0540
4	400	20.4	0.091	9	0.0591
5	500	20.4	0.50	9	0.0473
6	500	20.4	0.11	9	0.0550
7	400	10.2	0.89	9	0.0446
8	500	10.2	0.94	9	0.0580
9	500	30.0	0.96	9	0.0600
				Average	0.0526

It was found that the effective porosity was essentially constant (within experimental error) for either H_2 or CO as the contaminant (Table 3.1). The average value for the effective porosity from the H_2 tests was 0.0545 with a maximum deviation of 0.0119 and the average effective porosity from the CO tests was 0.0526 with a maximum deviation of 0.080. It is possible to have fairly large experimental errors in these tests since only 7-11 CuO pellets were used for each differential bed test. This is not enough pellets to insure a good statistical average since the individual pellets have a wide range of some of their physical properties (March 1961 Unit Operations monthly report).

3.2 Determination of Apparent Mass Transfer Factors for the H_2-CuO Reaction

In order to utilize the assumed mathematical model of external diffusion-internal diffusion of H_2 controlling the CuO-H_2 reaction, it is necessary to have available mass transport properties of the H_2 across the assumed external gas film surrounding the CuO pellet. These mass transport properties are usually presented as a mass transfer coefficient, k_g, which is used in the expression,

$$\text{rate of transport} = k_g a \, (C - C^*) \tag{2}$$

where

k_g = mass transfer coefficient, $\frac{\text{g-moles}}{\text{sec-cm}^2\text{-g-moles/cm}^3}$

a = external surface of the pellets, cm^2/cm^3

C = H_2 concentration in bulk gas, g-moles/cm^3

C^* = H_2 concentration at solid surface, g-moles/cm^3

k_g values are usually correlated as a function of the various physical properties of the system. The usual correlation is the mass transfer factor, J_D, as a function of Modified Reynold's Number, Re',

where

$$J_D = \frac{k_g \rho}{G} \left(\frac{\mu}{D \rho}\right)^{2/3} \tag{3}$$

$$Re' = \frac{D_P G}{\mu} \tag{4}$$

and

J_D = mass transfer factor, dimensionless

ρ = gas density at system conditions, g/cm^3

G = mass flow rate of gas stream, g/cm^2-sec

μ = viscosity of gas, poise or g/cm-sec

D = molecular diffusivity of H_2 in He, cm^2/sec

Re' = Modified Reynold's Number, dimensionless

D_p = mean surface diameter of CuO pellet, cm

There are numerous such correlations in the literature, however, the majority are at system conditions much different from the system of interest. In general, these correlations show that the J_D factor is dependent not only on Reynold's Number but also on particle size and the correlation goes thru a transition point between high and low Reynold's Numbers ($50 \leqq Re \geqq 150$) where the dependence on Reynold's Number changes.(1-8) All of the experimental tests on the H_2-CuO system were made at relatively low Modified Reynold's Numbers, < 15.0, where published correlations are varied and few in number. Rather than attempting to choose one particular correlation for use in this system, it was decided to determine the mass transfer factors for the range of operating conditions in this system from experimental data and develop a useable correlation. If this correlation falls in the range of published information, it would be further verification of the proposed mathematical model.

The mass transfer coefficients, k_g, were determined for each run by making a trial and error parameter search for k_g, utilizing a finite difference, machine solution of the proposed mathematical model (Unit Operations monthly report, May 1961).

Since the early part of the effluent hydrogen concentration curve for deep bed tests is influenced strongly by the hydrogen mass transfer through the gas film, the trial and error solution was made so that the predicted effluent hydrogen concentration was within 5% of the measured effluent hydrogen concentration at 20% of the run time necessary for the H_2 effluent concentration to reach 90% of the initial hydrogen concentration. This point was arbitrarily chosen so as to exclude the initial phase of each test where there was some data scatter.

From equations (3) and (4) and the calculated k_g values, a correlation of J_D vs Re' was made for the experimental system of interest (Figure 3.1). The resulting expression for the least squares fitted curve was:

$$J_D = 0.24\ (Re')^{-0.69} \qquad (5)$$

The resulting correlation is within the range of some of the published correlations although the slope of the J_D vs Re' plot is somewhat different. This correlation will be used in all future calculations for the deep bed tests.

References

1. Bar-Ilan, M., and Resnick, W., Ind. Eng. Chem. 49, 313 (1957).

2. Chu, Ju. Chin, Kalil, J., and Wetteroth, W. A., Chem. Eng. Prog. 49, 141 (1953).

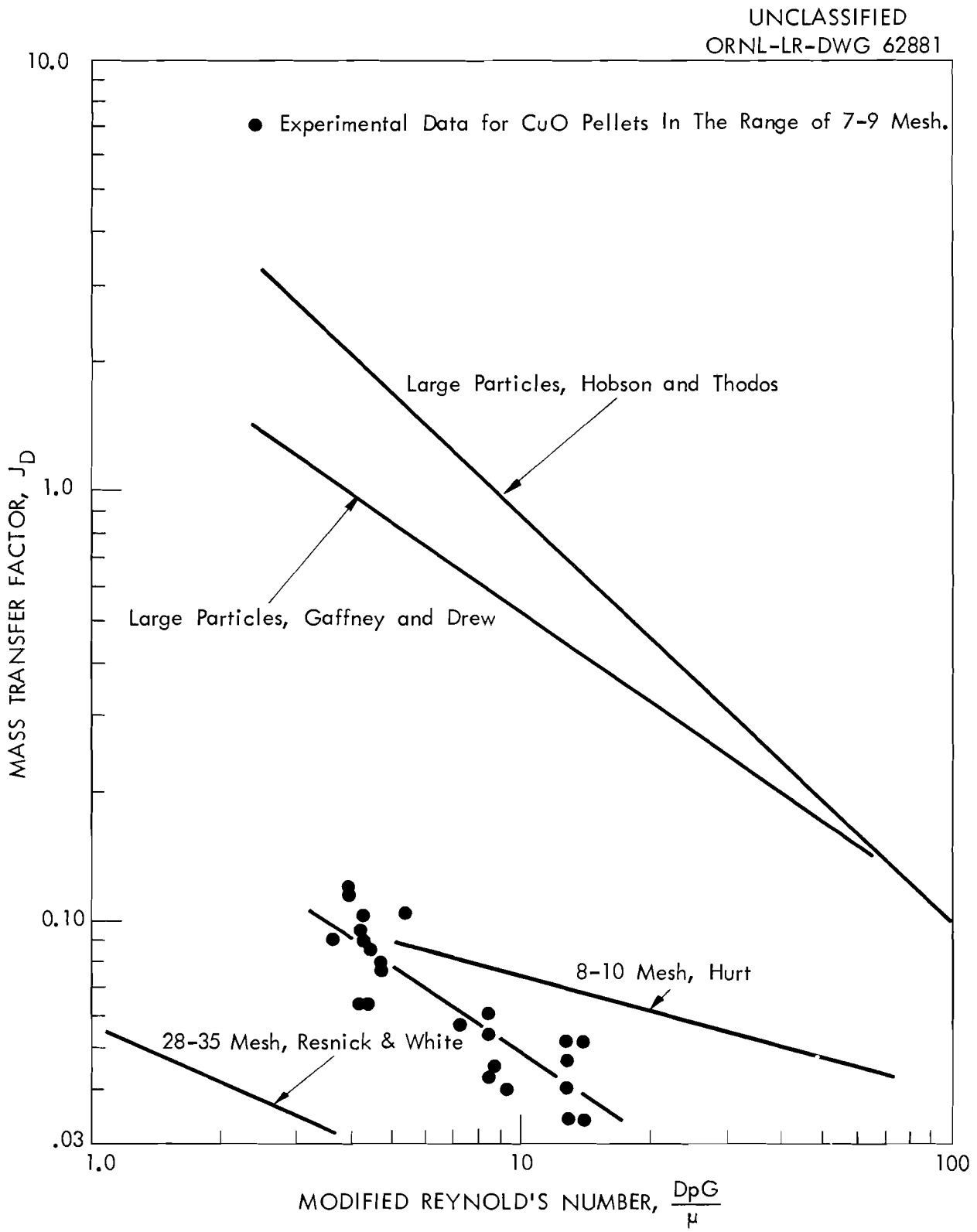

Fig. 3.1. J_D factor for mass transfer as a function of modified Reynold's number for the reaction, $H_2 + CuO = H_2O + Cu$.

3. Dryden, C. E., Strange, D. A., and Withrow, A. E., Chem. Eng. Prog., 49, 191 (1953).

4. Ergun, S., Chem. Eng. Prog. 48, 227 (1952).

5. Gaffney, B. J. and Drew, T. B., Ind. Eng. Chem. 42, 1120 (1950).

6. Hobson, M. and Thodas, G., Chem. Eng. Prog. 47, 370 (1951).

7. Hurt, D. M., Ind. Eng. Chem. 35, 522 (1943).

8. Resnick, W. and White, R. P., Chem. Eng. Prog. 45, 377 (1949).

4.0 POWER REACTOR FUEL PROCESSING

C. D. Watson

4.1 Modified Zirflex - F. G. Kitts

Modified Zirflex denotes a process for the recovery of uranium from U-Zr-Sn fuels by batchwise dissolution in NH_4F-NH_4NO_3-H_2O_2 solutions, stabilization with HNO_3-$Al(NO_3)_3$, and TBP extraction. During dissolution a small, continuous addition of hydrogen peroxide is made to oxidize U^{IV} to the more soluble U^{VI}. Such a process is desirable for processing zirconium fuels containing higher percentages of U (up to 10%) without the intermediate precipitation of UF_4 which would occur if no oxidant were added. Presently dissolutions of unirradiated zirconium fuels are being carried out both in a 1-in.-dia recirculating dissolver and in engineering-scale equipment.

Two runs (CZr-7 and 8) were made in the engineering-scale equipment dissolving 8% U-Zr plate (0.122-in. thick) in refluxing dissolvent initially 6.53 M NH_4F-0.15 M NH_4NO_3-0.01 M H_2O_2 with a continuous H_2O_2 addition at an average rate of 1-2 x 10^{-5} mols/cm^2-min (Table 4.1). In these runs and CZr-9 the H_2O_2 was introduced into the bulk of the boiling dissolvent through a water-cooled nozzle; this eliminated the gassing which had been observed at the H_2O_2 inlet. In run CZr-7 about 2.5 g of an apparently crystalline, green precipitate was collected which contained 60% U, 23% F and 6.4% Zr. Near the end of the run this material formed on the surface of the U-Zr and then dropped to the bottom of the dissolver; it is assumed to be the same material involved in the coat formation reported by Gens (ORNL-2905). After dilution of the dissolution product and standing for 24 hrs a fine white precipitate settled; this material (1.7224 g) contained 3.6% U (probably imparted by fines of the green material above) which represented a U loss of 0.15%. These materials had been produced in previous dissolutions but were not collected from the solvent extraction feeds because both were dissolved upon addition of the 1.8 M HNO_3 - 1.8 M $Al(NO_3)_3$ stabilizing solution. In run CZr-8, 9% more fluoride was charged (calculated terminal free F^-/U = 81 compared to 60 for CZr-7) and total dissolution was achieved in a shorter time (other conditions comparable) with only a trace of the green precipitate observed. Although different amounts of F^- were charged, equal terminal free F^-/U ratios of 82 were determined from experimental values; a lower free F^- would have been calculated had the Zr balance in run CZr-7 been ~95% rather than the 86.5% reported. Probably a target free F^-/U of 90 - 100 should be used to assure rapid dissolution and prevent coat and precipitate formation.

Run CZr-9 was made dissolving PWR seed plate ~2% U-Zr-Sn in 6.53 M NH_4F - 0.01 M H_2O_2. The amount of F^- charged was calculated to yield a terminal F^-/Zr ratio of ~6.8; this is about the lowest ratio which will yield a reasonable dissolution time. In this run about 2.6 g of a green-black precipitate was formed although the free F^-/U = 115. Some minimum free F^- concentration (a much lower free F^- gave a higher F^-/U here because the U was only 2% instead of 8%) may be required in the case of low U fuels, as well as the high F^-/U ratio required with high U fuels in order to accomplish total dissolution without precipitation.

Table 4.1. Data for Modified Zirflex Runs

Run No.	Dissolvent[a] Vol ℓ	Dissolvent[a] NH_4F M	Dissolvent[a] NH_4NO_3 M	U-Zr-Sn Fuel Plate Type	U-Zr-Sn Fuel Plate Wt g	U-Zr-Sn Fuel Plate Diss. %	U-Zr-Sn Fuel Plate Area cm^2	U-Zr-Sn Fuel Plate Thickness, in.	Diss. Time hrs	H_2O_2[g] Add Rate mols cm^2-min x 10^{-5}	Add H_2O Vol ℓ	Solvent Extraction Feed Vol ℓ	Solvent Extraction Feed Zr g/ℓ	Solvent Extraction Feed U g/ℓ	Solvent Extraction Feed F M	Solvent Extraction Feed Free F^-/U	Material Balances Zr %	Material Balances U %	Material Balances F %
CZr-7	6.42	6.53	0.15	8% U-Zr	517	99	519	0.122	3	1.2	5.7	12.35	33.3	2.9	3.19	82	86.5	86.6	94.3
CZr-8	7.0	6.53	0.15	8% U-Zr	515	100	517	0.122	2-1/4	2.0	7.3	14.315	32.3	2.65	3.04	82	97.6	92.1	95.2
CZr-9	6.75	6.53	0.0	PWR Seed	590	>99	862	0.081	4-2/3	1.1	4.19	11.09	51.3	1.03	3.87	6.88[c]	100.6[d]		97.5
	ml										ml	ml							
MZr-20	243	6.58	0.0	8% U-Zr	20.8	>99.9	23	0.122	2.4	0.93	87[e]	208	42.0	3.12[f]	3.81	80	92.1	85.5	100
											94	215	41.3	3.60	3.76	70			
MZr-21	248	6.58	0.0	8% U-Zr	20.8	>99.9	23	0.122	3.6	2.55	200	440	40.8	3.58	3.65	65	93.8	94.7	98.4
MZr-22	242	6.58	0.0	8% U-Zr	18.2	>99.9	20	0.122	1.4	2.0	267	500	33.4	2.81	3.13	79	99.9	96.6	98.1
MZr-23	287	6.58	0.0	PWR Seed	25.4	>99.9	46	0.081	4.2	0.84	160	456	53.1	1.71	4.13	7.16[c]	99.9[d]		99.5

Run No.	mols H_2 / mol Zr	mols NH_3 / mol Zr	Boil-up Rate ml / cm^2-min	NH_4OH in Reflux M	Scrubbed Off-Gas vol[b] ft^3	Scrubbed Off-Gas O_2 %	Scrubbed Off-Gas H_2 %	Scrubbed Off-Gas H_2O %
CZr-7	-	5.17	0.23	0.4-0.1	-	3.3	95	0.2
CZr-8	1.32	4.6	0.24	0.3-0.05	5.77	0.5-5.1	88-97	0.8-2.5
CZr-9	1.89	4.06	0.17	0.43-0.0	10.2	0.2-1.3	94-97	1-5

[a] Also contained 0.01 M H_2O_2.

[b] Metered at 25°C and 1 atm.

[c] F/Zr, Free F^-/U not controlling at low U.

[d] Combined weight balance given since U and Zr per centages not known accurately.

[e] Dissolution product divided into two equal parts and stabilized as shown.

[f] Precipitate formed - some U removed from solution.

[g] As 3-10% solution.

Probably the most significant finding of the recent work was the observation of the behavior of the O_2 concentration in the HNO_3-scrubbed off-gas (principally H_2). This variable is plotted as a function of refluxing time for runs CZr-8 and 9 in Figure 4.1. The O_2 concentration was reduced initially to < 0.1% by N_2 purging; the initial peak probably came from the decomposition of the 0.01 M H_2O_2 in the dissolvent. The concentration remained low during the period of rapid dissolution and then rose steadily as decomposition became the major mode of H_2O_2 destruction. This suggests that the H_2O_2 addition rate could be controlled to maintain the O_2 concentration in the off-gas at ~3 ± 2%. As much as 1% O_2 in the off-gas seems to indicate the presence of sufficient H_2O_2 to maintain U^{VI} in the dissolvent. While a reasonable excess of H_2O_2 is not harmful to dissolution, limiting the O_2 concentration in the off-gas to 5% avoids the flammable range (lower limit for O_2 in hydrogen is 6%).

Four runs (MZr-20, 21, 22 and 23, Table 4.1) were made in the 1-in.-dia recirculating dissolver to study solution stability and function as pilot runs for the larger equipment. Run MZr-20 was made with a calculated free F^-/U = 50; a small amount of green precipitate formed near the end of the run. Crystals formed in the more concentrated solvent extraction feed after ~36 hrs (before sampling), while the more dilute solution stood for about 30 days at room temperature before a small amount of crystals appeared. A small amount of precipitate again formed in the dissolution step of MZr-21 (calculated F^-/U = 55); however, a highly loaded, stable (no crystals after 36 days) SX feed was produced. Run MZr-22 at a calculated F^-/U = 81 produced no green precipitate; although the SX feed shown in Table 4.1 (vol = 500 ml) was stable (no crystals after 30 days), crystals formed in < 24 hrs when it was first diluted to a volume of 475 ml. An additional 25 ml of water dissolved the crystals and produced a stable solution. Run MZr-23 was made under the same calculated terminal conditions (F^-/Zr = 6.8) as run CZr-9 in the engineering-scale equipment but no green precipitate formed in the small scale dissolver. The U-Zr-Sn material dissolved in the small run contained 1.6 times as much U as that used in the large scale run resulting in a much lower free F^-/U (88 compared to 115 for the cell run) but a higher free F^- (F^-/Zr = 7.10 compared to 6.88) since less Zr was present for F^- complexing. (The initial fluoride charge was calculated: F^- = 6.8 [total wt U-Zr-Sn/91.22]). This observation strengthens the hypothesis that some minimum free fluoride concentration (~1 M in the dissolution product) must be maintained as well as free $F^-/U \geq 90$ in order to prevent U precipitation during dissolution.

4.2 Shearing and Leaching - B. C. Finney

A chop and leach program to determine the economic and technological feasibility of continuously leaching the core material (UO_2 or UO_2-ThO_2) from relatively short sections (1-in. long) of fuel elements produced by shearing is continuing. This processing method enjoys the apparent advantage of recovering fissile and fertile material from spent power reactor fuel elements without dissolution of the inert jacketing material and end adaptors. These unfueled portions are stored directly in a minimum volume as solid waste. A "cold" chop-leach complex consisting of a shear, conveyor, leacher, and compactor is being evaluated prior to "hot" runs.

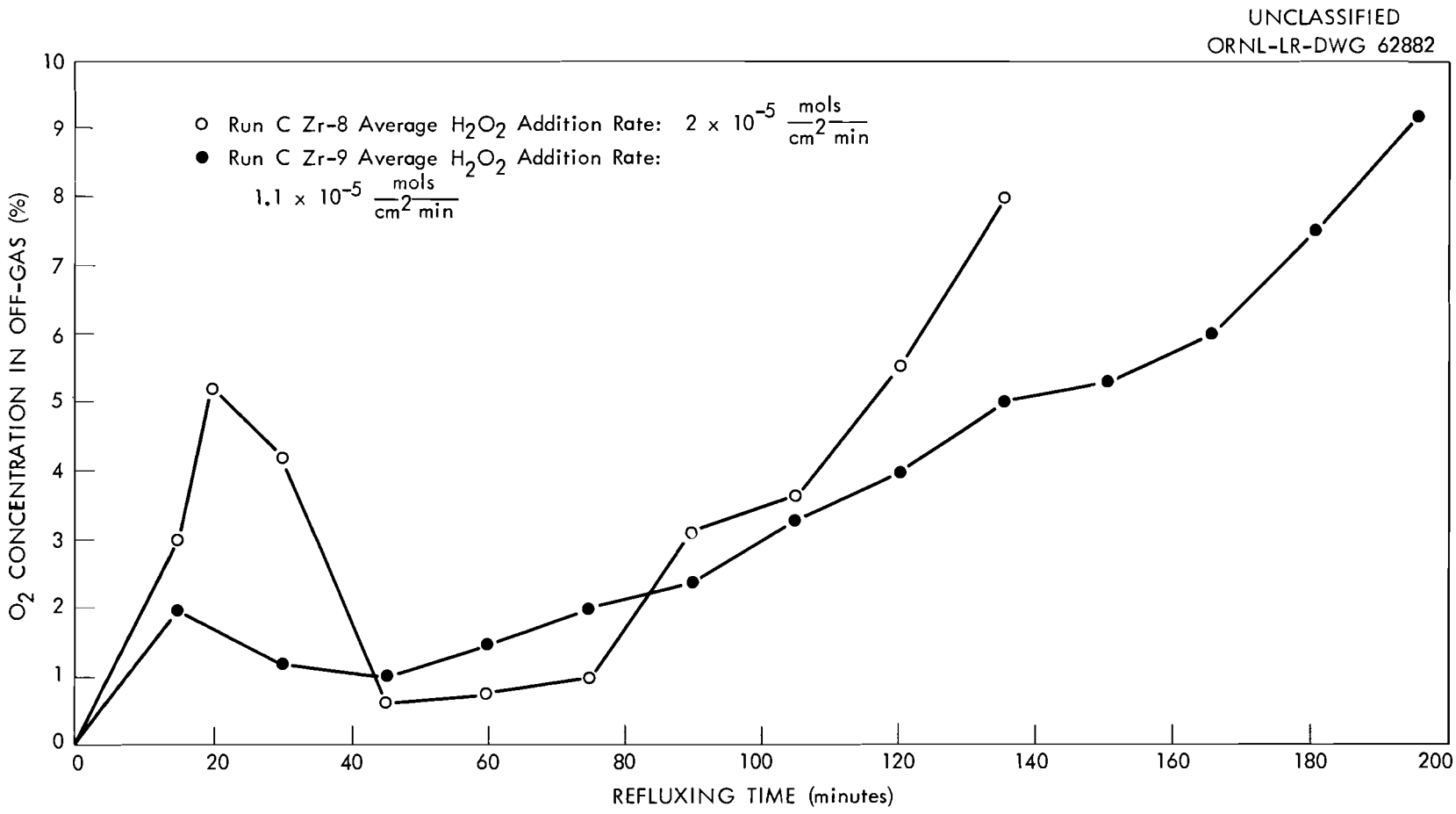

Fig. 4.1. Oxygen concentration in scrubbed off-gas as a function of refluxing time.

Shear. The 250 ton shear including the hydraulic system and feed mechanism has been received from the Birdsboro Corp. Installation of the shear and auxiliary equipment on the third floor of Bldg. 4505 has begun.

Eleven Mark I-Model 7 fuel assemblies have been filled with Davison Chemical Co. UO_2 pellets. Each assembly contains ~4000 pellets weighing ~60 kg.

Conveyor. The conveyor has been received from the Weld Craft Co. of Dayton, Ohio. Slight modifications will be made to the inner drum to eliminate the gaps between the flights and inner cylinder and the inner cylinder will be filled with linear-polyethylene for criticality control.

Leacher. Four leaching runs were made in the 4 stage pyrex glass leacher model (Table 4.2). The fuel charge consisted of chopped stainless steel clad UO_2 (1/2-in.-OD x 1-in. long) and 6, 7, and 8 M HNO_3 was used as the dissolvent.

Run 28 was a scouting run in which one batch of chopped stainless steel clad UO_2 containing 437.8 g of UO_2 was leached with 8 M HNO_3. The purpose of this run was to determine the operability of the leacher model when leaching the very fine UO_2 from the chopped stainless steel sections. The results of this run indicated that there would be no difficulty encountered in the operation of the model and as a consequence three leaching runs (run 29, 30, and 31) were made in which the UO_2 was leached from 9 batches of chopped stainless steel clad UO_2.

In each run there was some variation in the weight of UO_2 per batch (Table 4.2). The 9 flasks were charged with a similar volume of weighed chopped sections and at the conclusion of each run the empty cladding was weighed and the amount of UO_2 per batch determined by difference.

The product incremental uranium loading and acidity as represented by the sections of the curves above line A-B for runs 29, 30, and 31 are presented in Figures 4.2, 4.3, and 4.4. In each run a fresh batch of chopped sections was put on stream every hour. A comparison of the maximum, minimum and composite product uranium loading and acidity of runs 29, 30, and 31 are presented in the following table:

Run No.	Dissolvent M HNO_3	Product: Uranium Loading, g/liter Max	Min	Composite	Acidity, M HNO_3 Max	Min	Composite
29	8	670	30	425	7.5	0.5	3.0
30	6	670	35	325	5.5	0.1	2.5
31	7	615	60	350	6.2	0.1	3.0

In each run 60 - 90 min were required to completely leach the UO_2 from the chopped sections.

Table 4.2. Leacher Model Dissolution Data UO_2-HNO_3 System

Charge: Chopped sections of stainless steel clad UO_2, ~(1/2-in.-OD x 1-in.-long)

Run No.	UO_2 Batch No.	Dissolution Time min	Temp, °C	Dissolvent (HNO_3) M	Dissolvent (HNO_3) Flow Rate ml/min	Dissolvent (HNO_3) Vol liters	UO_2 Wt Charged g	UO_2 % Dissolved	Product (Composite) Loading g U/liter	Product (Composite) H^+ M	Product (Composite) Vol liters	Off-gas Nitrogen g-mol	Off-gas % of HNO_3 Feed	Acid Consumption g-mol HNO_3 / g-mol UO_2
28	1	90	102-111	8	18.6	1.67	437.8	100	236	5.24	1.62	0.97	7.2	2.6
29	1	240	101-111	8	18.8	12.39	478	100	304	4.45	12.4	7.47	7.65	2.47
	2	240	102-111				490	100						
	3	240	102-111				495	100						
	4	240	102-111				472	100						
	5	240	101-111				479	100						
	6	240	102-110				466	100						
	7	240	101-110				480	100						
	8	240	101-110				401	100						
	9	240	102-111				524	100						
30	1	240	101-107	6	25.4	15.24	501	100	258	3.19	15.1	9.5	10.4	2.58
	2	240	102-107				496	100						
	3	240	101-107				512	100						
	4	240	102-108				491	100						
	5	240	101-108				502	100						
	6	240	102-108				479	100						
	7	240	101-107				474	100						
	8	240	102-108				496	100						
	9	240	102-108				473	100						
31	1	240	101-109	7	21.0	13.64	494	100	299	3.84	13.6	9.13	9.56	2.56
	2	240	103-109				490	100						
	3	240	101-109				479	100						
	4	240	102-109				520	100						
	5	240	103-109				478	100						
	6	240	103-109				481	100						
	7	240	102-109				485	100						
	8	240	100-108				487	100						
	9	240	100-109				504	100						

UNCLASSIFIED
ORNL-LR-DWG 62883

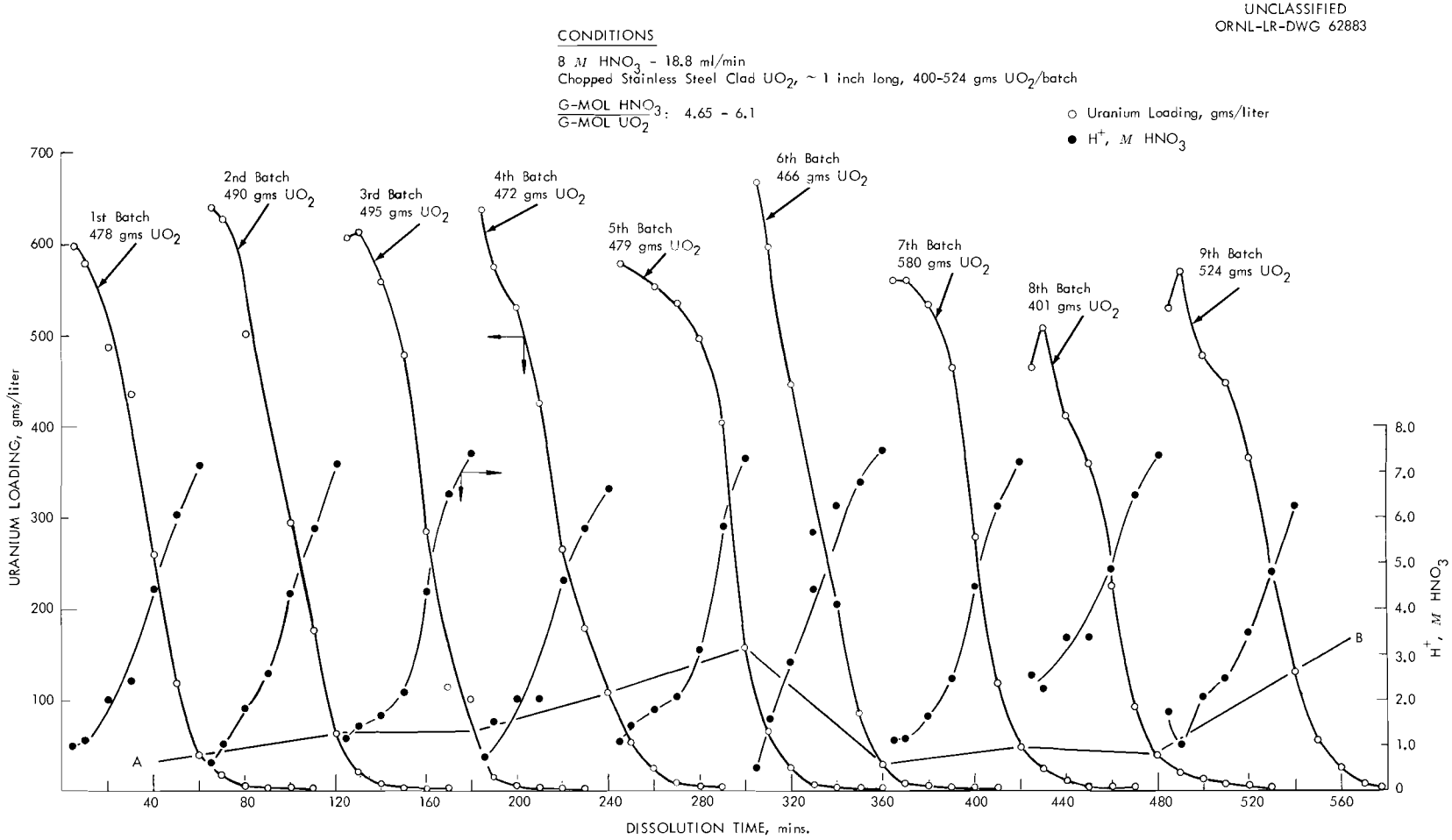

Fig. 4.2. Uranium loading and H^+ as a function of dissolution time for the leaching of 9 batches of chopped stainless steel clad UO_2 (Run-29) in the 4 stage leacher model based on a 4 hour dissolution time.

UNCLASSIFIED
ORNL-LR-DWG 62884

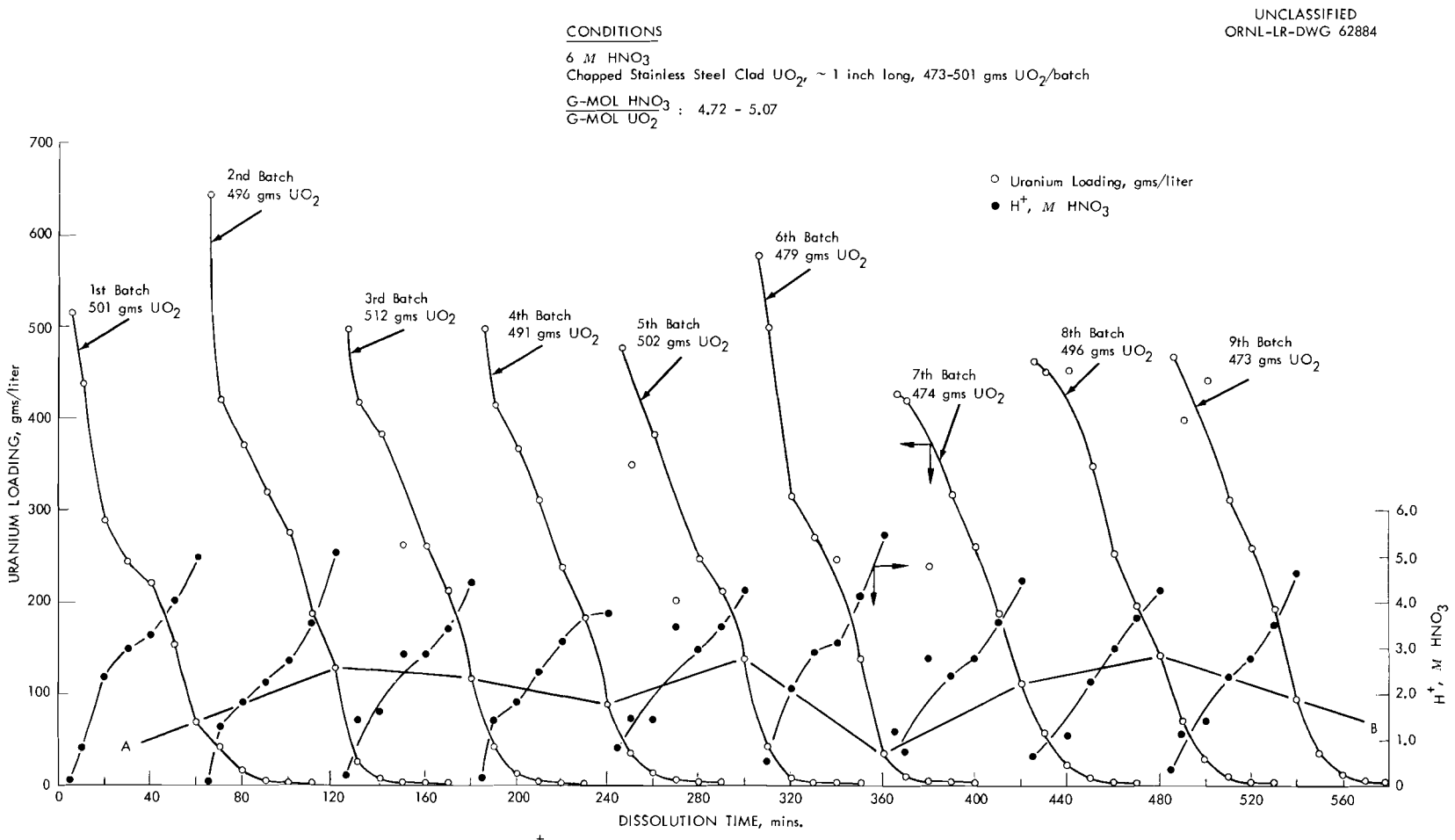

Fig. 4.3. Uranium loading and H^+ as a function of dissolution time for the leaching of 9 batches of chopped stainless steel clad UO_2 (Run-30) in the 4 stage leacher model based on a 4 hour dissolution time.

UNCLASSIFIED
ORNL-LR-DWG 62885

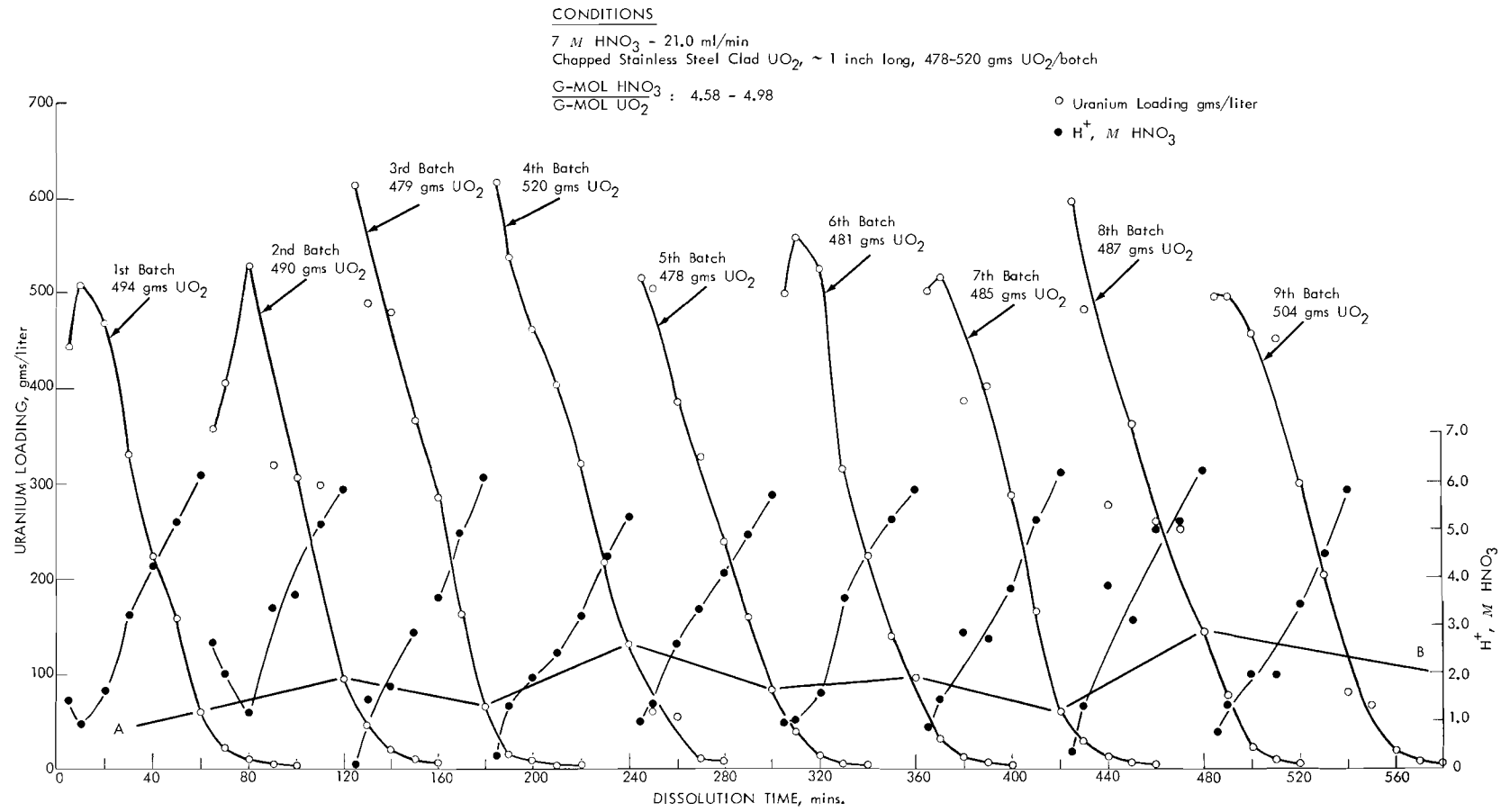

Fig. 4.4. Uranium loading and H^+ as a function of dissolution time for the leaching of 9 batches of chopped stainless steel clad UO_2 (Run-31) in the 4 stage leacher model based on a 4 haur dissalution time.

5.0 REACTOR EVALUATION STUDIES

J. C. Suddath

5.1 Heat Transfer from Spent Fuel Elements during Shipping - J. S. Watson

Initial efforts have been made to analyze experimental data on temperature rises in electrically heated mock fuel elements contained within simulated shipping carriers. The apparatus used in these studies has been described previously (Unit Operations April 1961 monthly progress report). The first approach has been to calculate the temperatures expected within the fuel bundle if radiation were the only method of heat transfer inside the carrier. Thus far calculations have only been made using approximate but conservative estimates of the radiation factors within the bundle. The resulting temperatures predicted by these calculations have been surprisingly close to those observed experimentally within the bundles.

In general, the net radiant flux from a surface 1 to a surface 2 is calculated from relations of the form

$$\frac{Q}{A_1} = A_2 \mathcal{F}_{12} \sigma \left(T_1^4 - T_2^4\right) \qquad (1)$$

where

σ = Stefan-Boltzman constant

T_1, T_2 = absolute temperatures of tubes 1 and 2

Q = net radiation from 1 to 2

A_1, A_2 = areas of 1 and 2

$\mathcal{F}_{12}$ = radiation factor for 1 to 2

The problem in using this relation arises because $\mathcal{F}_{12}$ is a rather complicated function of the areas, emissivities, and configuration factors not only for radiation between tubes 1 and 2 but between all surfaces in the system. $\mathcal{F}_{12}$ must account for all of the heat from tube 1 which is sorbed by tube 2 and some reaches tube 2 through complicated multiple reflections from surrounding tubes.

Efforts are being made to evaluate the radiation factors in the manner described by McAdams[1] and credited to Hottel. However, until these efforts yield positive results, an approximate system has been used which is believed to give conservative values for $\mathcal{F}$'s. Essentially a special case of the McAdams treatment was used where one assumes that 1 and 2 are the only source-sink surfaces. All other tubes are no flux surfaces. If one considers a tube near the center of the bundle, all tubes surrounding 1 and 2 have the same area and emissivity, ϵ, and the radiation factor is obtained by[1]

---

[1] McAdams, Heat Transmission, 3rd Ed. McGraw-Hill (1954), pp. 72-76.

$$\mathcal{F}_{12} = \frac{1}{\frac{1}{\overline{F}_{12}} + \left(\frac{1}{\epsilon} - 1\right)} \tag{2}$$

$\overline{\mathcal{F}}$ is defined by the relation[2]

$$\overline{F}_{12} = F_{12} + F_{1R} \frac{F_{R2}}{1 - F_{RR}} \geqslant \mathcal{F}_{12}$$

where R represents the no flux surfaces surrounding 1 and 2. For more conservative values of $\mathcal{F}_{12}$, $\overline{F}_{12}$ was taken equal to F_{12}. This essentially neglects any heat going to 2 from R. These simplications in $\mathcal{F}$'s also simplify temperature calculations within the bundle because the configuration factor between any two tubes is only a function of their relative position (adjacent, diagonal, etc.) and not a function of their position in the bundle.

For power reactor fuels, the tubes are generally spaced very close together, and each tube can "see" and, with the above simplifications, radiate to no more than four adjacent tubes, four diagonal tubes, and either other tubes which are located adjacent to the diagonal tubes in the square pitched array. All of the heat generated within a given tube must be (net) radiated to these 16 tubes. Then the total net heat radiated, Q_i, from tube i will be

$$Q_i = A\sigma \sum_{j=1}^{16} \frac{T_i^4 - T_j^4}{\frac{1}{F_{ij}} + 2\left(\frac{1}{\epsilon} - 1\right)} \tag{3}$$

A relation such as this can be written for each tube in the fuel bundle, and these equations (linear in T^4) can be solved simultaneously for each T_n^4. For large tube bundles of varying size, a rapidly convergent trial and error procedure for the equations appeared simpler than a procedure for setting up and evaluating the determinates for direct solution of the equations.

Equation (3) can be solved directly for T_i^4 to give

$$T_i^4 = \sum_{j=1}^{16} \left[\frac{1}{F_{ij}} + 2\left(\frac{1}{\epsilon} - 1\right)\right] \left[\frac{Q_i}{A\sigma} + \sum_{j=1}^{16} \frac{T_j^4}{\frac{1}{F_{ij}} + 2\left(\frac{1}{\epsilon} - 1\right)}\right] \tag{4}$$

The first summation is the same for all tubes.

$$\sum_{j=1}^{16} \left[\frac{1}{F_{ij}} + 2\left(\frac{1}{\epsilon} - 1\right)\right] = \frac{4}{F_1} + \frac{4}{F_2} + \frac{8}{F_3} + 32\left(\frac{1}{\epsilon} - 1\right)$$

---

[2] Ibid, p. 71.

where

F_1 = configuration factor for radiation to an adjacent tube

F_2 = configuration factor for radiation to a diagonal tube

and F_3 = configuration factor for radiation to a tube adjacent to a diagonal

In the trial and error procedure, all tubes were initially set at the carrier wall temperature and then the temperature required for each tube to radiate its generated heat was calculated from equation (4) and assigned to that tube. The calculations were repeated throughout the bundle until the center tube temperature changed by less than 0.01°C.

A slight complication arises in the outer two rows of tubes of the bundle since these tubes radiate part of their energy to the cast wall and not to other tubes. Rather than directly evaluating configuration factors for radiation to the wall and using difficult equations, other than (4), for these tubes, it was simpler to simulate the case wall by considering two imaginary rows of tubes, whose temperatures were set at the wall temperature, completely surrounding the bundle. These tubes should affect the calculations much like the wall but still allow one to proceed completely through the bundle using the same equation for resetting the tube temperatures.

Some reduction in computation can be obtained by noting that the temperatures within the bundle will by symetrical. Although one needs only evaluate the temperatures in one octant of the bundle, one must always carry temperatures of tubes of at least two rows removed from the octant. For machine calculations the testing and control statements necessary take away most of the advantage of calculating the temperatures of less than one-half of the tubes.

These calculations were made (with the IBM-7090) for the conditions employed in some of the experimental runs (Tables 5.1, 5.2, and 5.3). The wall temperature of the simulated carrier was not constant for any of the experiments, but it varied with the angle from vertical (Figure 5.1). For the calculations, an average value was used. The agreement of the results with the experimental results was surprisingly good, especially at higher heat generation rates. The average deviation of the experimental temperatures and the calculated temperatures (only 19 of the 36 tube temperatures were measured and could be used in the average) were 16, 19, and 22°C, respectively, for the three runs shown in Tables 5.1, 5.2, and 5.3 with heat generation rates of 0.0986, 0.0708, and 0.0481 watts/cm. One would expect all calculated temperatures to be equal to or higher than the measured temperatures if all of the constants employed were correct. This was not always the case, and although the calculated temperatures were higher on the average, this still throws some questions on the results.

There were very apparent effects of convection in the experimental data which will need to be taken into account. First, the radial dependence of the cast wall temperature was apparently caused by the convective "chimney" above the bundle. Also because of convection the measured temperature distribution was not symetrical. The temperatures in the upper half of the bundle were notably higher than those in the lower half. Methods of accounting for and correlating the effects of convection are being considered.

Table 5.1. Calculated and Experimental Temperature Distribution in an Enclosed 36-Tube Bundle

1-1 163.48 [193]	1-2 188.69 [238]	1-3 198.80 [223]	1-4 198.80 [225]	1-5 188.70	1-6 163.48
2-1 188.69 [205]	2-2 222.35 [227]	2-3 236.04 [248]	2-4 236.04	2-5 222.35	2-6 188.70
3-1 198.80	3-2 236.04	3-3 251.22 [243]	3-4 251.22 [240]	3-5 236.04 [232]	3-6 198.80 [189]
4-1 198.80	4-2 236.04	4-3 251.22 [234]	4-4 251.22 [234]	4-5 236.04 [222]	4-6 198.80 [187]
5-1 188.70	5-2 222.35	5-3 236.04	5-4 236.04	5-5 222.35 [206]	5-6 188.70 [166]
6-1 163.48	6-2 188.70	6-3 198.80	6-4 198.80	6-5 188.70 [184]	6-6 163.48 [167]

Q = 0.0986 watts/cm

Average wall temperature = 73.0°C

Emissivity = 0.55

[ ] Experimentally measured temperature

Difference between calculated and measured temperature = 16°C

Table 5.2. Calculated and Experimental Temperature Distribution in an Enclosed 36-Tube Bundle

1-1 135.24 [152]	1-2 157.48 [171]	1-3 166.44 [178]	1-4 166.44 [179]	1-5 157.48	1-6 135.24
2-1 157.48 [159]	2-2 187.44 [177]	2-3 199.69 [194]	2-4 199.69	2-5 187.44	2-6 157.48
3-1 166.44	3-2 199.69	3-3 213.33 [188]	3-4 213.33 [185]	3-5 199.70 [180]	3-6 166.45 [145]
4-1 166.44	4-2 199.69	4-3 213.33 [180]	4-4 213.33 [182]	4-5 199.70 [170]	4-6 166.45 [142]
5-1 157.48	5-2 187.44	5-3 199.70	5-4 199.70	5-5 187.44 [157]	5-6 157.48 [127]
6-1 135.24	6-2 157.48	6-3 166.45	6-4 166.45	6-5 157.48 [140]	6-6 135.24 [128]

Q = 0.0708 watts/cm

Average wall temperature = 58.0°C

Emissivity = 0.55

[ ] Experimentally measured temperature

Difference between calculated and measured temperature = 19°C

Table 5.3. Calculated and Experimental Temperature Distribution in an Enclosed 36-Tube Bundle

1-1 110.36 [116]	1-2 128.78 [130]	1-3 136.30 [137]	1-4 136.30 [138]	1-5 128.78	1-6 110.36
2-1 128.78 [122]	2-2 154.06 [134]	2-3 164.53 [148]	2-4 164.53	2-5 154.06	2-6 128.78
3-1 136.30	3-2 164.53	3-3 176.25 [142]	3-4 176.25 [141]	3-5 164.53 [136]	3-6 136.30 [111]
4-1 136.30	4-2 164.53	4-3 176.25 [136]	4-4 176.25 [137]	4-5 164.53 [128]	4-6 136.30 [109]
5-1 128.78	5-2 154.06	5-3 164.53	5-4 164.53	5-5 154.07 [119]	5-6 128.78 [98]
6-1 110.36	6-2 128.78	6-3 136.30	6-4 136.30	6-5 128.78 [107]	6-6 110.36 [99]

Q = 0.0481 watts/cm

Average wall temperature = 50.0°C

Emissivity = 0.55

[ ] Experimentally measured temperature

Difference between calculated and measured temperature = 22°C

UNCLASSIFIED
ORNL-LR-DWG 62886

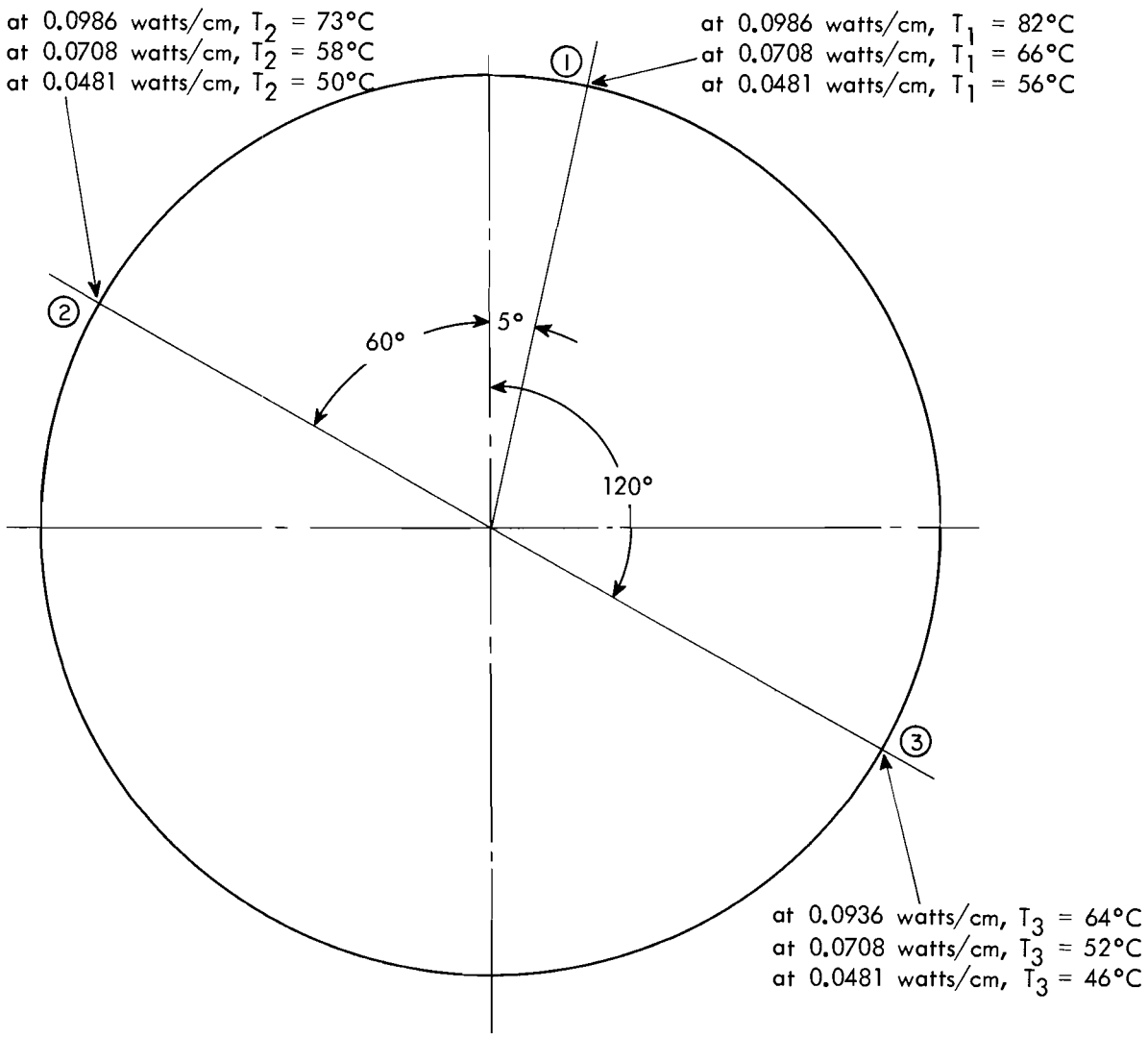

Fig. 5.1. Angular wall temperature distribution on simulated spent fuel shipping carrier wall.

6.0 SOLVENT EXTRACTION STUDIES

A. D. Ryon

The HETS values for uranium stripping reported this month were obtained using the 5% TBP flowsheet described in the September Unit Operations Monthly Progress Report (CF 60-9-43).

6.1 HETS Values for Uranium Stripping in Sieve and Nozzle Plate Pulse Columns - R. S. Lowrie, F. L. Daley

HETS values were obtained for the aqueous continuous operation of the 12 ft sieve plate column (0.125-in.-dia holes, 23% free area) and for both aqueous and solvent continuous operation of the 12 ft nozzle plate column (0.125-in.-dia nozzles, 10% free area with the nozzles facing down).

Operating conditions were those for the 5% TBP flowsheet, a Purex type flowsheet employing 5% TBP in Amsco 125-82 as the solvent and 0.01 M nitric acid as the strip reagent. Loaded solvent for the test was obtained as a continuous flow from an extraction column. The experimental conditions for the test are shown in Table 6.1, the average analytical results for the flowing streams and column profile samples in Tables 6.2 and 6.3 and the uranium distribution curves for 5% TBP and several acid concentrations in Figure 6.1. HETS values were calculated using the number of theoretical stages determined from a McCabe-Thiele diagram (Figure 6.1 is a typical diagram). In order to minimize the effect of increased analytical error at low uranium concentrations, HETS values based on analysis of less than 0.01 g/liter uranium were not calculated. The solvent uranium concentrations were used for all HETS calculations for stripping regardless of which phase was continuous in the column. This necessitated calculating solvent values for aqueous continuous runs by material balance (Table 6.3). The most representative HETS values (Table 6.4) for aqueous continuous operation of the sieve plate column were 2.2 ft at 50 cpm and 2.4 ft at 70 cpm for a 6 ft length of column. HETS values for aqueous continuous operation of the nozzle plate column remained constant at 3.1 ft as the pulse frequency increased from 30 to 50 cpm for a 9 ft length of column. Solvent continuous operation of the nozzle plate column showed that the HETS values decreased from 2.0 to 1.7 ft as the pulse frequency increased from 50 to 90 cpm for a 6 ft length of column. In all cases, 12 ft of column was sufficient to reduce the uranium concentration in the stripped solvent stream to 0.005 g/liter or less, equivalent to a uranium loss of < 0.1%.

Several tests were made with a solvent to aqueous ratio of ~7. Although the operating line and equilibrium lines were too close to permit the calculation of HETS values, in all cases, the uranium loss in the stripped solvent stream was < 0.1%.

Table 6.1. Experimental Conditions for 5% TBP Uranium Stripping Tests

Run No.	Column Cartridge	Pulse Frequency cpm	Continuous Phase	Flow Rates gal ft^{-2} hr^{-1} Solvent	Strip	Total	Ratio O/A	% Flooding
1	S	50	Aq	343	74.6	418	4.6	90
2	S	70	Aq	248	51.6	300	4.8	> 95
5	N	50	Solv	344	75.3	419	4.6	45
6	N	70	Solv	256	63.1	319	4.1	60
7	N	90	Solv	131	29.4	160	4.5	80
8	N	50	Aq	134	29.5	164	4.5	60
9	N	30	Aq	341	74.4	415	4.6	> 95

S - Sieve plates 0.125-in.-dia holes, 23% free area
N - Nozzle plates 0.125-in.-dia nozzles, 10% free area

Pulse amplitude = 1 inch

Table 6.2. Average Analytical Data for Flowing Streams

Run No.	Loaded Solvent U g/ℓ	H^+ M	Aqueous Product U g/ℓ	H^+ M	Stripped Solvent U g/ℓ	H^+ M	% U Acct for
1	8.00	0.03	37.0	0.20	< 0.001	< 0.01	100.6
2	7.99	0.05	34.7	0.22	< 0.001	< 0.01	90.3
5	7.95	0.09	33.6	0.25	0.005	0.08	92.6
6	7.47	0.10	33.9	0.22	< 0.001	0.01	111.8
7	7.97	0.10	32.2	0.21	< 0.001	< 0.01	90.6
8	7.27	0.10	30.9	0.21	0.003	< 0.01	93.6
9	8.20	0.04	34.0	0.20	0.003	< 0.01	90.6

Table 6.3. Average Analyses of Profile Samples

Location of Sample Points - Feet from Bottom

Run No.	+3 Aqueous U g/ℓ	+3 Aqueous H^+ M	+3 Actual Solvent U g/ℓ	+3 Actual Solvent H^+ M	+3 Calculated Solvent* U g/ℓ	+3 Calculated Solvent* H^+ M	+6 Aqueous U g/ℓ	+6 Aqueous H^+ M	+6 Actual Solvent U g/ℓ	+6 Actual Solvent H^+ M	+6 Calculated Solvent* U g/ℓ	+6 Calculated Solvent* H^+ M	+9 Aqueous U g/ℓ	+9 Aqueous H^+ M	+9 Actual Solvent U g/ℓ	+9 Actual Solvent H^+ M	+9 Calculated Solvent* U g/ℓ	+9 Calculated Solvent* H^+ M
1	-	-	-	-	-	-	0.94	< 0.01	0.045	< 0.01	0.022	< 0.01	-	-	-	-	-	-
2	-	-	-	-	-	-	0.82	0.02	0.007	< 0.01	0.017	< 0.01	-	-	-	-	-	-
5	4.47	0.10	0.77	0.02	-	-	0.317	0.05	0.053	0.03	-	-	0.066	0.06	0.005	0.02	-	-
6	2.67	0.02	0.110	0.01	-	-	0.057	0.01	0.007	0.01	-	-	0.022	0.05	< 0.001	0.01	-	-
7	7.49	0.05	0.164	0.01	-	-	0.22	0.01	0.007	0.01	-	-	0.026	0.04	< 0.001	0.01	-	-
8	8.46	0.13	1.09	0.01	1.86	< 0.01	0.99	0.02	0.105	< 0.01	0.219	< 0.01	0.122	0.02	0.012	< 0.01	0.029	< 0.01
9	10.3	0.09	0.628	< 0.01	2.21	< 0.01	0.69	0.02	0.014	< 0.01	0.160	< 0.01	0.015	0.02	0.003	< 0.01	0.006	< 0.01

* Calculated by material balance from aqueous values.

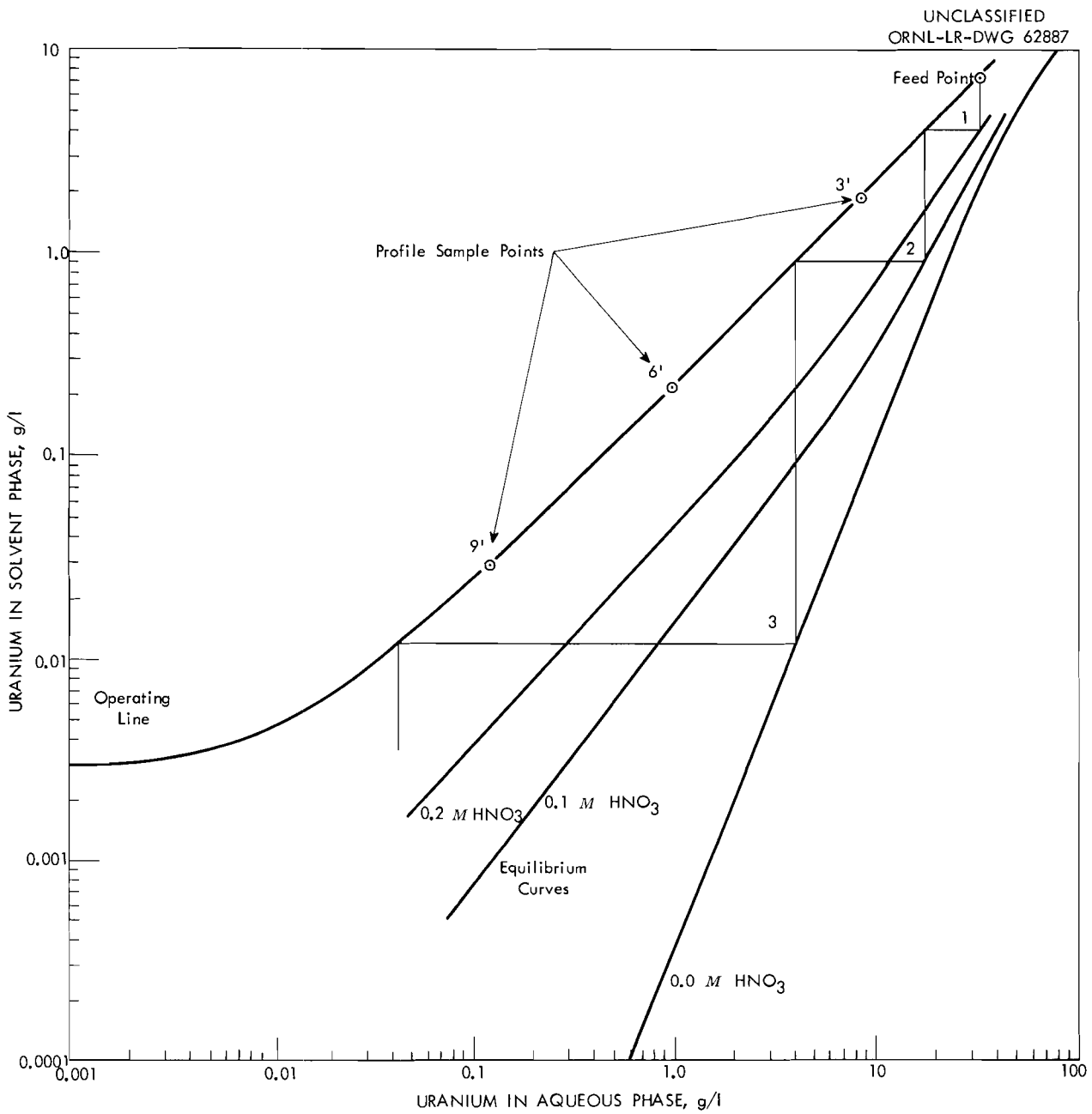

Fig. 6.1. McCabe-Thiele diagram for stripping uranium from 5% TBP - Run 8.

Table 6.4. HETS Values for Stripping Uranium from 5% TBP-Amsco

Run No.	Continuous Phase	Pulse Frequency cpm	Phase Ratio O/A	HETS Values - Feet: Location of Column Section Above Feed Point - Feet 0-3	0-6	0-9	3-6	3-9	6-9
Sieve Plate Column (0.125-in.-dia holes, 23% free area)									
1	Aq	50	4.6	-	2.2	-	-	-	-
2	Aq	70	4.8	-	2.4	-	-	-	-
Nozzle Plate Column (0.125-in.-dia nozzles, 10% free area)									
5	Solv	50	4.6	1.3	2.0	-	3.2	-	-
6	Solv	70	4.1	1.0	1.7	-	3.2	-	-
7	Solv	90	4.5	1.2	1.7	-	3.1	-	-
8	Aq	50	4.5	1.8	2.2	3.1	3.3	3.7	3.4
9	Aq	30	4.6	1.8	2.1	3.1	3.2	3.5	3.3

7.0 VOLATILITY

R. W. Horton

7.1 MSR Core Fuel Reprocessing - W. W. Pitt

The core fuel salt for the proposed Molten Salt Breeder Reactor will be a mixture of Li^7F and BeF_2 plus $U^{235}F_4$ and possibly ThF_4. The accumulation of fission products in this salt will necessitate processing at frequent intervals to remove accumulated neutron absorbing poisons. The processing scheme[1] currently under consideration involves separation of U^{235} from the salt by the volatility process and recovery of the high cost Li^7F and BeF_2 from the residue (Figure 7.1).

The salt recovery process consists of dissolution of the salt in liquid HF, followed by a solids separation step to remove insoluble F.P. fluorides, and then finally evaporation of the HF leaving purified salt. Laboratory studies of the dissolution of lithium and beryllium fluorides in HF have indicated that the rate of dissolution is greatly increased by agitation or by increasing the surface to volume ratio. This, in addition to a need for a continuous process, led to the consideration of spraying as a means of introducing salt into liquid HF.

Due to the difficulties experienced at Argonne National Laboratory[2] with single phase nozzles spraying fused salts, a two phase or atomizing nozzle was chosen for study.

Spray Nozzle Performance Specifications. A maximum mean particle diameter of 50 microns was chosen to maintain the high surface volume ratio required for rapid dissolution of salt in HF. The nozzle must maintain the salt fluid (~ 550°C) until it is discharged. Because the salt is highly contaminated the nozzle must be simple and reliable or easily replaced remotely. The nozzle will have to handle varying rates of fused salt; the mean rate will be about 3 gal/hr.

Pressure Nozzles. In pressure nozzles the fluid is under pressure and is broken up by its inherent instability and its impact on the atmosphere. Here the energy required to break the fluid into small drops is supplied only by that stored in the fluid under pressure. To produce droplets about 50 microns would require pressures greater than 60 psi in the fused salt system and nozzle diameter less than 0.020 inches which would tend to plug.

Rotating Nozzles. In rotating nozzles the fluid is fed at low pressure to the center of a rapidly rotating disk or cup. Centrifugal force causes the fluid to be broken up into drops. This type nozzle would be highly subject to bearing failure in the corrosive atmosphere of the fused salt, HF system. Also there would be the difficulty of keeping the salt molten while it was on the disk.

Two Fluid Atomizing Nozzles. In atomizing nozzles the fluid is subject to a high-velocity jet of gas which supplies the energy required to break it up into fine droplets. In this type nozzle there are no moving parts to fail, the fused salt nozzle can be of fairly large diameter with required pressure less than 20 psi, and it may be readily heated by resistance heating.

UNCLASSIFIED
ORNL-LR-DWG 62888

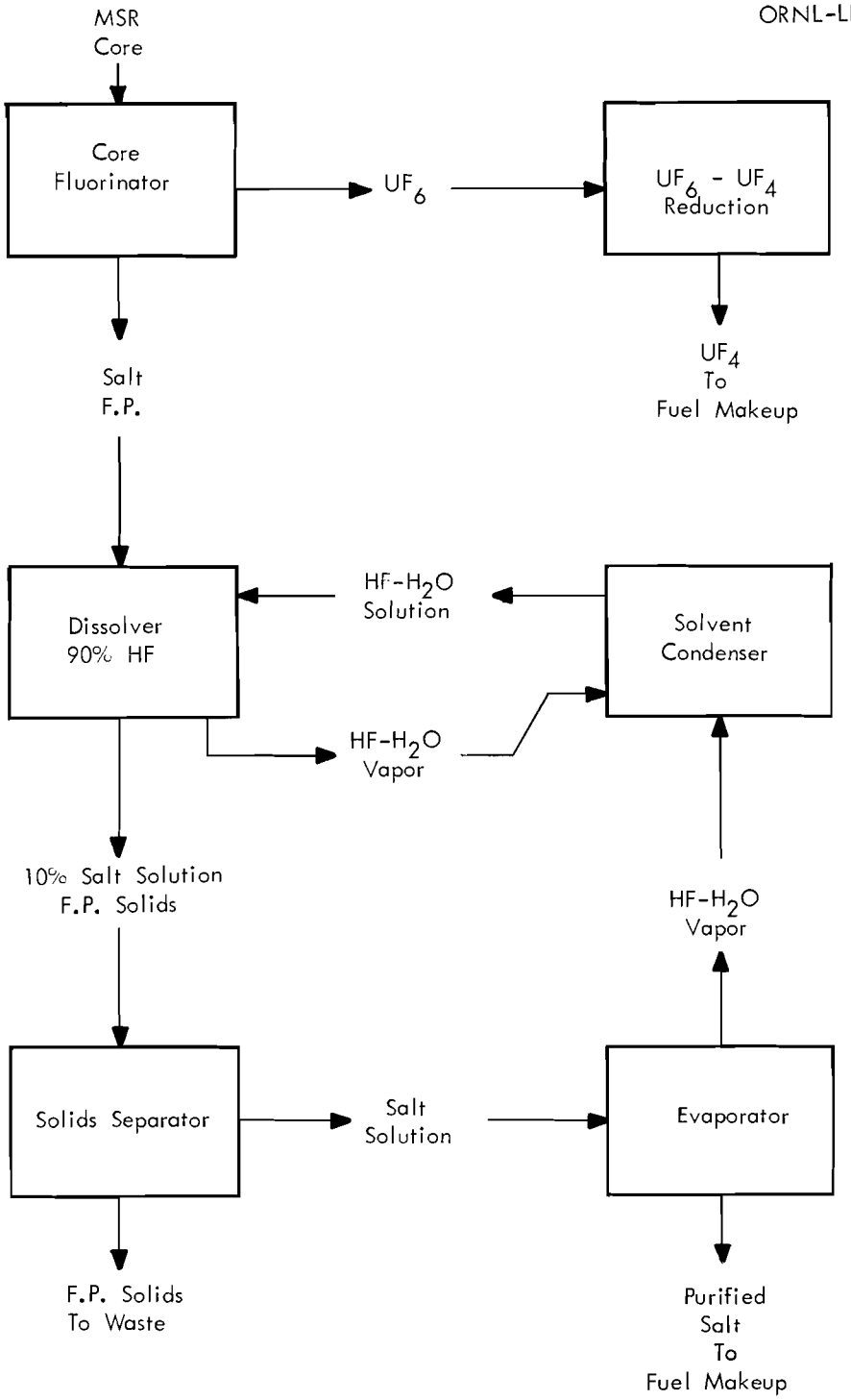

Fig. 7.1. Proposed flowsheet for MSR core fuel processing.

The problems associated with this nozzle type, that of supplying a large volume of high velocity gas and of separating the small salt particles from the gas, may be solved with present technology.

Two-Fluid Atomizer Sizing Calculations. The two fluid atomizer equations developed by Nukiyama and Tanasawa,[3] were used.

$$D = \frac{15{,}930\sqrt{\sigma}}{V_a\sqrt{\rho\ L}} + 191\left(\frac{\mu}{\sqrt{\rho\ L\ \sigma}}\right)^{0.45}\left(\frac{1000\ Q_L}{Q_A}\right)^{1.5} \qquad (1)$$

where

σ = surface tension of liquid, dynes/cm

μ = viscosity of liquid - centipoises

ρ = liquid density - lb/ft^3

Q_L, Q_A = volumetric flow rates of liquid and air, respectively, ft^3/sec

V_a = relative velocity between two fluids - ft/sec

D = mean droplet diameter - microns

For calculations the following physical constants of the fused salt were assumed:

σ = 180 dynes/cm

μ = 8.4 centipoises

ρ = 134 lb/ft^3

The selected diameter of the fused salt nozzle was 25 mils. It was felt that this approached the minimum diameter through which fused salt would easily flow. If the salt driving force through the nozzle is 20 psi, the salt velocity will be

$$V_L = 0.6\sqrt{\frac{2g_c\Delta P}{\rho}} = 0.6\sqrt{\frac{64.3 \times 20 \times 144}{134}} = 22 \text{ ft/sec}$$

From equation (1), it is apparent V_a must be much greater than 400 ft/sec, for D to be less than 50 microns. Therefore V_A must be greater than 500 ft/sec. Also from equation (1), it is apparent that Q_A must be on the order of $5000/Q_L$.

$$Q_L = \frac{22 \cdot \pi}{144}\left(\frac{0.025}{2}\right)^2 = 7.5 \times 10^{-5} \text{ ft}^3/\text{sec}$$

$$Q_A = 5000 \cdot 7.5 \times 10^{-5} = 0.375 \text{ ft}^3/\text{sec}$$

Area of gas nozzle = 0.375/500 x 144 = 0.11 in.^{2}

Where the outside diameter of salt nozzle is 1/4-in. the ID of gas nozzle must be 0.63-in.

Nozzle Heating and Construction Details (Figure 7.2). To prevent the fused salt from freezing in the nozzle and plugging it, a means of heating the nozzle to greater than 500°C must be provided. The best way of doing this is by resistance heating the nozzle. This requires a continuous electrical circuit through the nozzle. The salt nozzle was machined from Inconel bar stock, to a wall thickness of ~32 mils, (the same as small tubing), and an inner diameter of 25 mils at the discharge end (Figure 7.3). The inlet of the nozzle was welded to the 1/4-in. Inconel transfer line. The discharge end to 1/2-in. Inconel tubing which circumscribed the transfer line for about 10-in. and terminated at an Inconel ring joint flange. Two Chromel Alumel thermocouples were attached to the inner wall of the annulus, one at the nozzle tip, and the other about 4 inches from the tip. The annulus was filled with magnesium oxide insulation to prevent short circuiting. This provided an electrical path from the flange, which was insulated from the ground, through the 1/2-in. tubing, nozzle, 1/4-in. transfer line, supply tank to ground. The resistance of this circuit was approximately 0.2 ohms.

The atomizing gas was fed through 1-in. Inconel tubing which was concentric to the 1/2-in. tubing for about 5 in. It was tapered to 0.6-in. at the outlet, just beyond the nozzle tip. This provided parallel flow of the two fluids. The gas supply tubing was bent 90°, to allow the salt line to enter in a straight line, through an opening cut in the 1-in. tubing. A ring joint flange welded to the bend, perpendicular to the discharge section, allowed the salt nozzle and the gas supply line to be disconnected. A section of 1/2-in. pipe sealed the inner flange to the 1-in. tubing.

Molten Salt Supply Tank and Transfer System. To provide a supply of molten salt, a tank was made from 6-in. Schedule 40 Inconel pipe, and 1 in. plate. This tank was heated to 800°C in an 8-in. Hevi-duty furnace, and pressurized to 30 psi with nitrogen to provide the driving force for transfer of the molten salt. The salt was transferred through 1/4-in. Inconel tubing wrapped with asbestos insulation tape. The 10 ft of transfer line and nozzle were resistance heated by 100 amp current at 18 volts potential. This provided a temperature of approximately 700°C in the transfer line and > 850°C in the nozzle, before flow of atomizing air.

Atomizer Testing. The atomizer shown in Figure 7.4 was first tested with water and air. The sprayed water droplets were caught in molten paraffin and examined optically. With a water flow of approximately 0.5 cu ft/hr and an air flow of approximately 5000 cu ft/hr droplets of 5 - 100 micron in diameter were obtained, with a mean less than 25 microns. From equation (1) and the physical constants of water and fused salt, it is apparent that for a given flow of the two fluids the mean droplet diameter of fused salt should be approximately twice that for water. Therefore with a fused salt flow of 0.5 cu ft/hr and an air flow of 5000 cu ft/hr a mean droplet diameter of < 50 microns should be obtained.

UNCLASSIFIED
ORNL-LR-DWG 62889

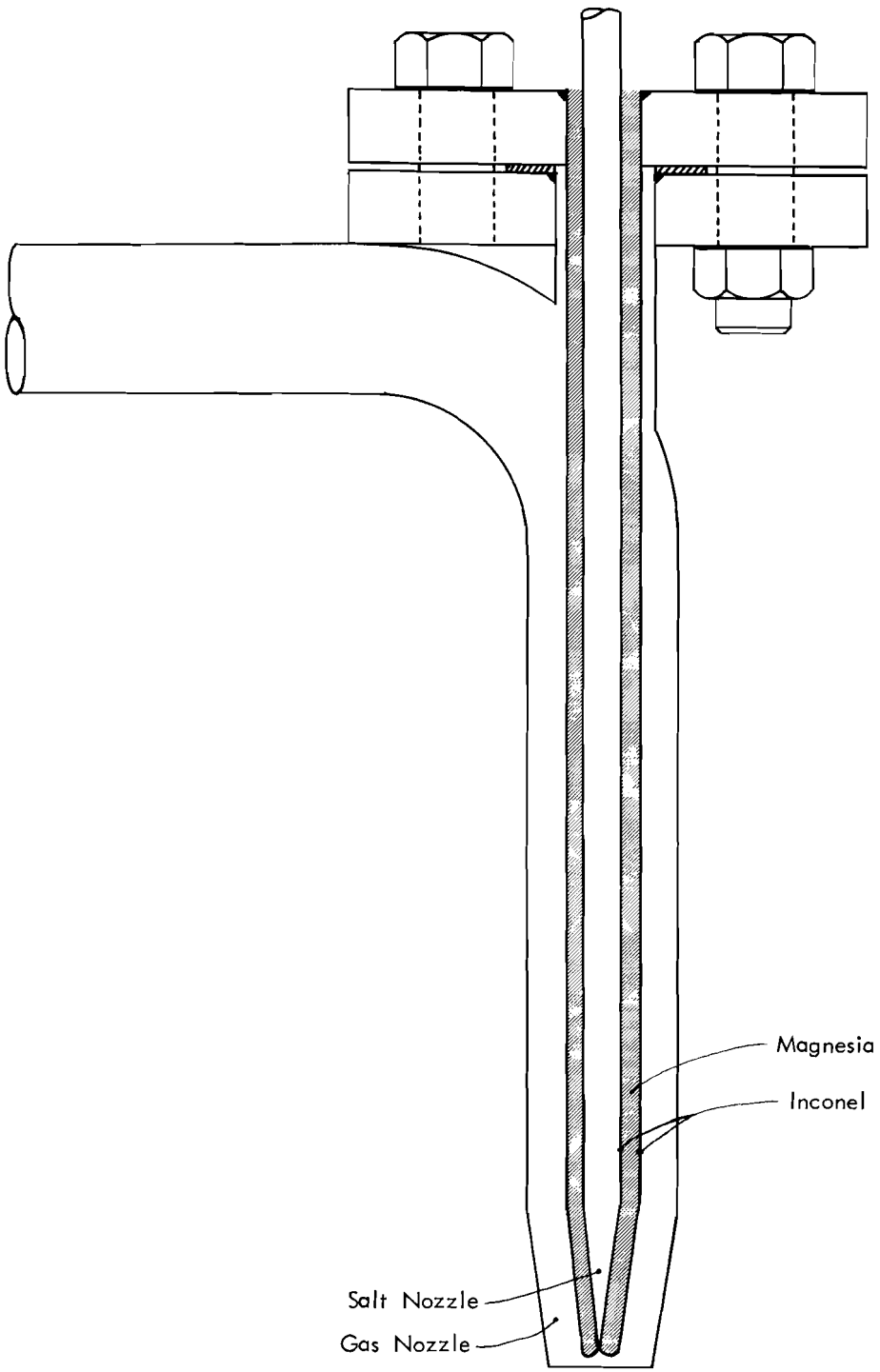

Fig. 7.2. Molten salt atomizer.

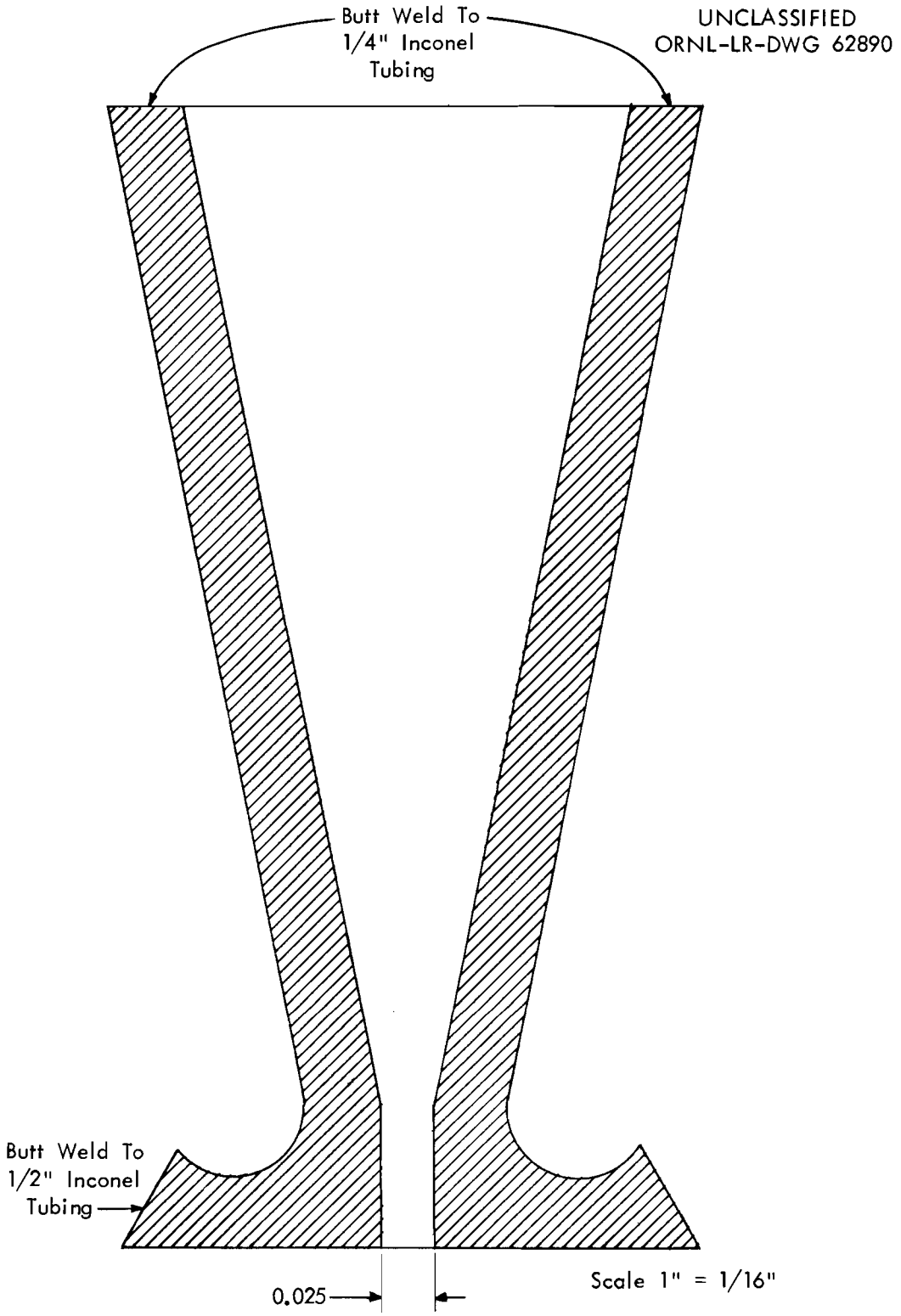

Fig. 7.3. Fused salt nozzle.

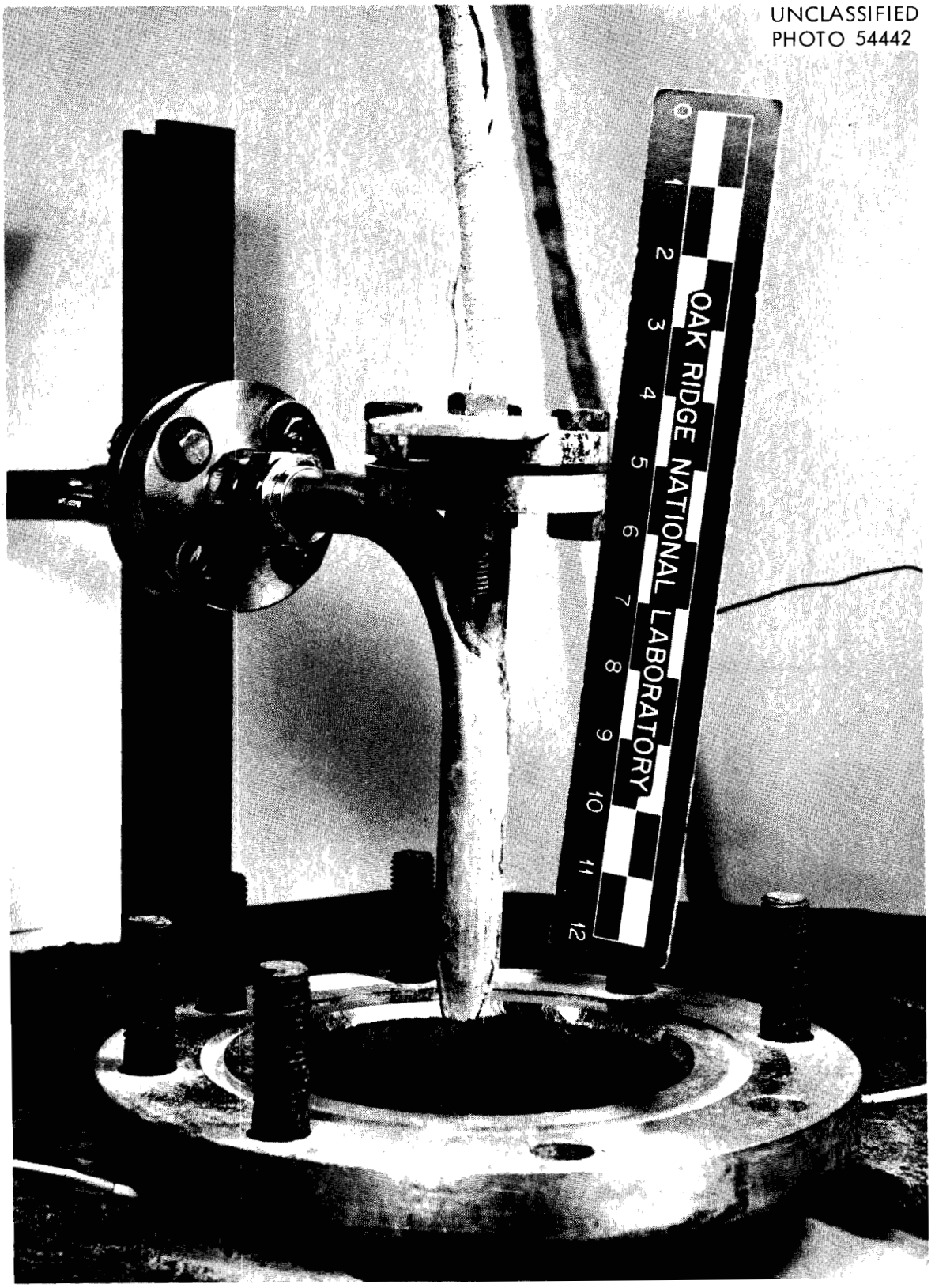

Fig. 7.4. Two fluid atomizing nozzle.

The nozzle was then welded to the 1/4-in. transfer line, and resistance heating circuit connected. After charging the supply tank with 26-42-32 mol % Na-Li-Zr F salt, the salt was fused and an attempt made to spray it. Though the nozzle and transfer line temperatures were greater than 700°C, no salt was sprayed after a 3 hr effort. Later visual inspection showed that salt had been transferred to the tip of the nozzle. After drilling the nozzle out with a 0.025 in. drill, a second attempt was made, and this time salt was successfully sprayed for 15 min at a rate of 0.3 cu ft/hr. Atomization was not continuous, however, because a cake of frozen salt built up around the salt nozzle when the atomizing air was on. This would quickly break away when the air was turned off, so the nozzle was operated as an atomizer in cycles.

The sprayed salt was collected in water which separated the solids from the high velocity air. A 5 gallon open container was placed in an open 55 gal drum (Figure 7.5), and both had approximately 4 in. of water. This way the non-atomized salt was retained in the 5 gal container only.

Results. Samples of sprayed salt were taken from both the 5 gal container and the 55 gal drum. In addition, samples of dry salt were taken from surfaces near the nozzle where the salt had settled out.

Microscopic examination of the samples showed that those samples which had been wet by water were mostly irregular particles < 5 microns in diameter (Figure 7.6a). Those collected dry were mostly spheres 25 - 100 microns in diameter (Figure 7.6b). However, the existence of sub-micron spheres indicates the atomizing nozzle may produce some droplets in this range (Figure 7.7).

Conclusions - Continuous Dissolution. It appears to be very feasible to obtain a mean droplet diameter of < 75 microns by atomizing fused salt. The fact that the particles of salt which were sprayed into water were much smaller and much more irregular than the droplets collected dry, indicates that the droplets had been apparently shattered into very fine particles by rapid cooling. This suggests that a small droplet diameter is not necessary (even the salt which was not atomized was collected as very small, irregular particles). For continuous dissolution in HF, it should only be necessary to introduce molten salt in a fine stream into liquid HF.

The two major problems in atomizing fused salt are the supply of a large volume of high velocity atomizing gas (probably very corrosive) and the separation of the solid salt droplets from the atomizing gas. Neither of these problems should be too difficult to solve.

Continuous Fluorination. As a result of the preliminary tests of fused salt atomization, spray fluorination should be reconsidered as a continuous process for recovery of uranium from fused salt in the volatility process. The disadvantages listed by Gabor, et al.,[2] should be somewhat overcome by the use of an atomizing nozzle.

1. The fused salt nozzle diameter is not critical to the atomization, thus fewer nozzle replacements would be required.

2. The use of fluorine as the atomizing gas and the very small droplets obtained should provide high recovery in one cycle.

UNCLASSIFIED
ORNL-LR-DWG 62891

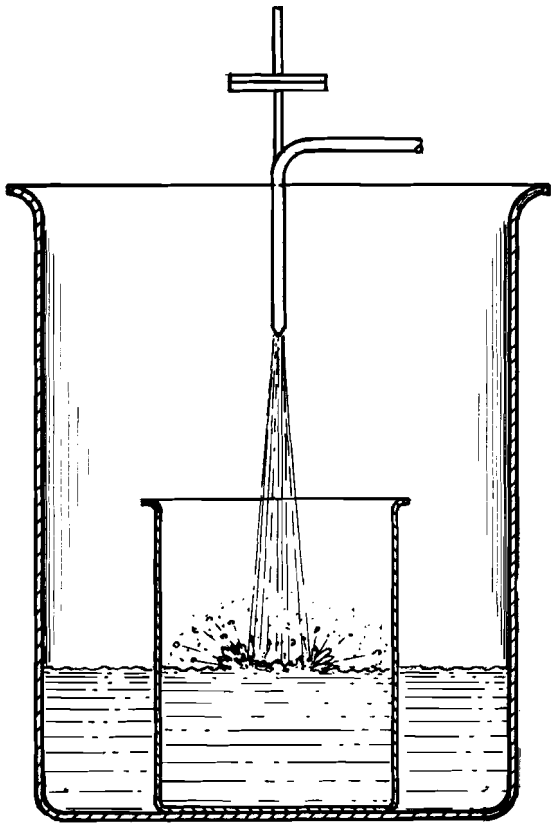

A - Non-Atomized

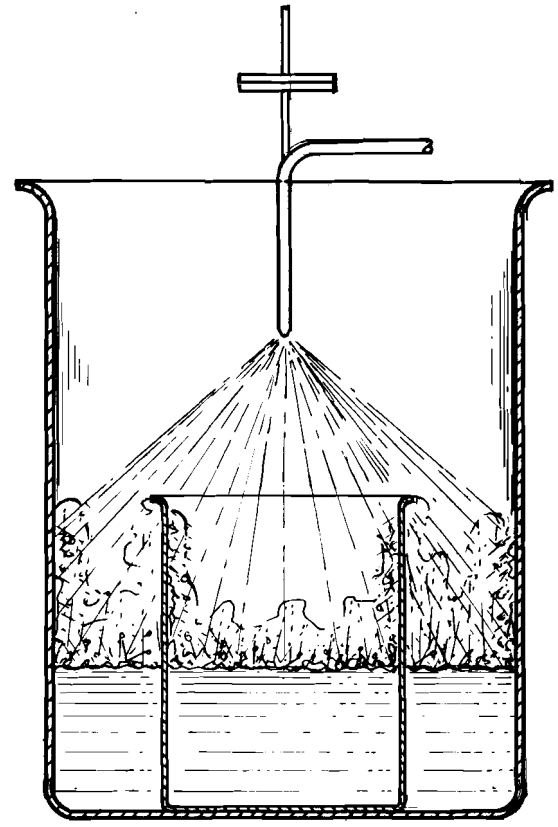

B - Atomized

Fig. 7.5. Salt Collection.

UNCLASSIFIED
PEM-3263-3

A. Salt Quenched by Water

UNCLASSIFIED
M-2997

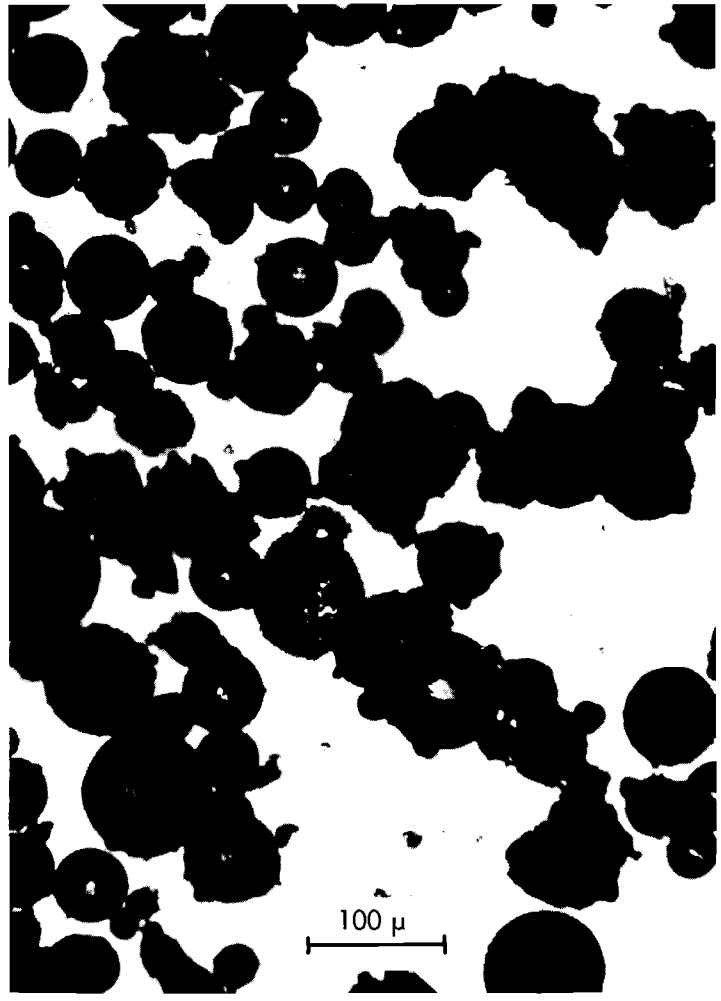

B. Salt Collected Dry

Fig. 7.6. Atomized salt.

UNCLASSIFIED
PEM-3263-1

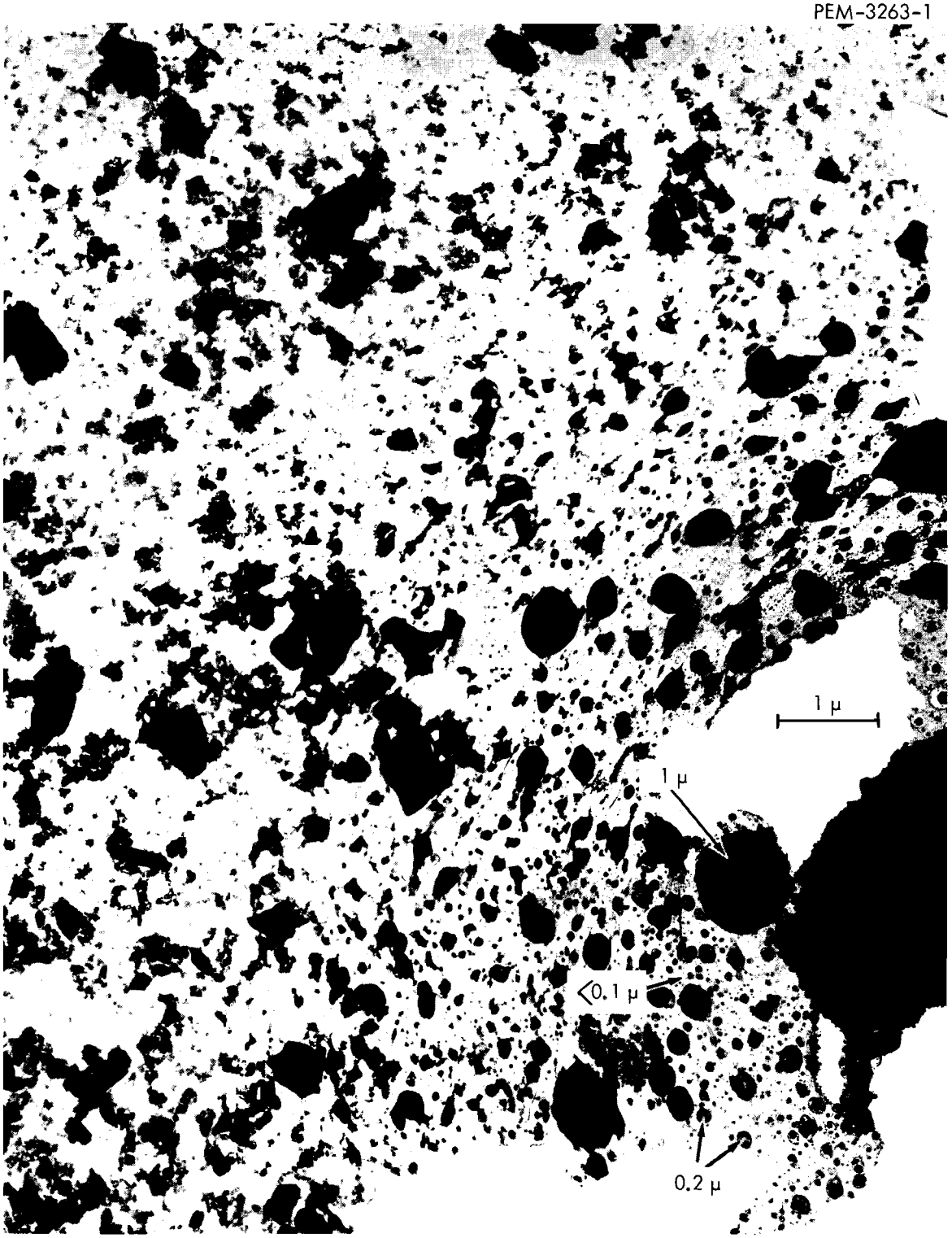

Fig. 7.7. Atomized salt quenched in water particularly note sub micron spheres.

References

1. Campbell, D. O. and Cathers, G. I., "Processing of Molten Salt Power Reactor Fuels," Ind. and Eng. Chem., Vol. 52, p. 41, January 1960.

2. Gabor, J. D., Mecham, W. J., Jonke, A. A. and Rodger, W. A., "Spray Fluorination of Fused Salt as a Uranium Recovery Process," ANL-6131.

3. Nukiyama, S. and Tanasawa, Y., "Trans. Soc. Mec. Engrs.," (Japan) 4, No. 14, 86 and No. 15, 138 (1938); 5, No. 18, 63 and 68 (1939); 6 No. 22 II-7 and No. 15, 138 II-8 (1940).

8.0 WASTE PROCESSING

J. C. Suddath

The purpose of this program is to obtain engineering information for the design of a hot pilot plant, which will demonstrate the disposal of high level waste solutions. Since the hot pilot plant may be built at the Idaho Chemical Processing site where TBP-25 waste is available, TBP-25 waste of the composition stored at Idaho was used for this test.

8.1 Evaporator-Calciner Test (R-38) - C. W. Hancher

Test R-38 was operated using the same procedure as was used for test R-37 reported in the May 1961 Unit Operations Monthly Report. The close coupled evaporator-calciner was operated and controlled as reported for test R-37. The feed for this test was TBP-25, simulated from the sampled composition of tank WM-182 at the Idaho Chemical Processing Plant, Table 8.1. Cold Ru was added to check its volatility during the evaporation-calcination operation.

The average feed rate for the test was 27.6 liters for an hour, Table 8.2, Figure 8.1. Only 89% of the nitrate was accounted for, while the ruthenium and mercury balances were 45% and 42%. The unaccounted for ruthenium and mercury are probably plated as solid in the off-gas system. However, the mercury did concentrate in the evaporator during the standby period, Table 8.3.

8.2 Evaporator-Calciner Control and Operation

Test R-38 started with the evaporator filled with cold feed and the calciner empty and cold (Table 8.4). The evaporator contents were heated to boiling and then the calciner was heated and filled simultaneously, requiring about 60 min to fill. As the control variables reached their set point values they were switched from manual to automatic control. The control settings for five controlled streams are shown in Tables 8.5 and 8.6. The system controlled satisfactorily for over 90% of the time. The evaporator level (Figure 8.2) was within control limits at all times, except when the level probe plugged. This caused feed to foam over into the condensate tank.

The control of variables has been evaluated by the setting of limits:

Limit "A" Too high, out of control, dangerous
Limit "B" Upper limit of good control
Limit "C" Lower limit of good control
Limit "D" Too low, out of control, uneconomical

The evaporator density exceeded only limit "B" during the operational period of the test. When the calciner was filled about the 13 hour the feed rate to the calciner decreased to a low rate, the evaporator was put on standby, no more feed was added to the system. As the calciner demanded feed at a low rate the Al^{+++} concentration of the evaporator decreased, Figure 8.3. The temperature of the evaporator controlled satisfactorily, but acid concentration of the evaporator did not follow the temperature

Table 8.1. Test R-38 Feed Concentration - "TBP-25"

	H molar	Al M	Hg g/liter	HNO_3 M	Fe g/liter	Na g/liter	Ru g/liter
As made up*	1.26	1.72	4.0	6.6	0.16	2.4	
As analyzed							
Tank 1	1.75	1.7	5.75	6.6	0.20		0.148
Tank 2	1.48	1.7	4.60	6.6	0.31		0.148
Tank 3	1.70	1.7	4.31	6.6	0.31		0.158

* Concentration of Tank - WM-182, Idaho Chemical Processing Plant

Table 8.2. System Balances and Results

	Test R-38	TBP-25 Waste
Nitrate Balance		
Input	2917 g moles	
Recovery		
(condensate	2581 g moles	88.5%
(solid	3 g moles	0.1%
(off-gas	6 g moles	0.2%
		88.8%
Ruthenium Balance		
Input	66.5 g	
Recovery		
(condensate	0.9 g	1.3%
(solid	28.5 g	43.0%
(evaporator	0.8 g	1.1%
		45.4%
Mercury Balance		
Input	2250 g	
Recovery		
(condensate	17 g	0.7%
(solid	89 g	3.9%
(evaporator	840 g	37.0%
		41.6%

Off-gas

1260 cu ft total
1152 cu ft leakage and purge
108 cu ft non-condensable (74 cu ft oxygen)

108/442 = 0.245 cu ft/liter of system feed

Average Feed Rate

442/16 hr = 27.6 liter/hr average

(11 + 5 at low rate)

Water Feed Rate

1457 liter of water, water to feed ratio = 3.3

Calcined Solids

38 kg solid/68 liters = 0.56 g/cc Bulk Density

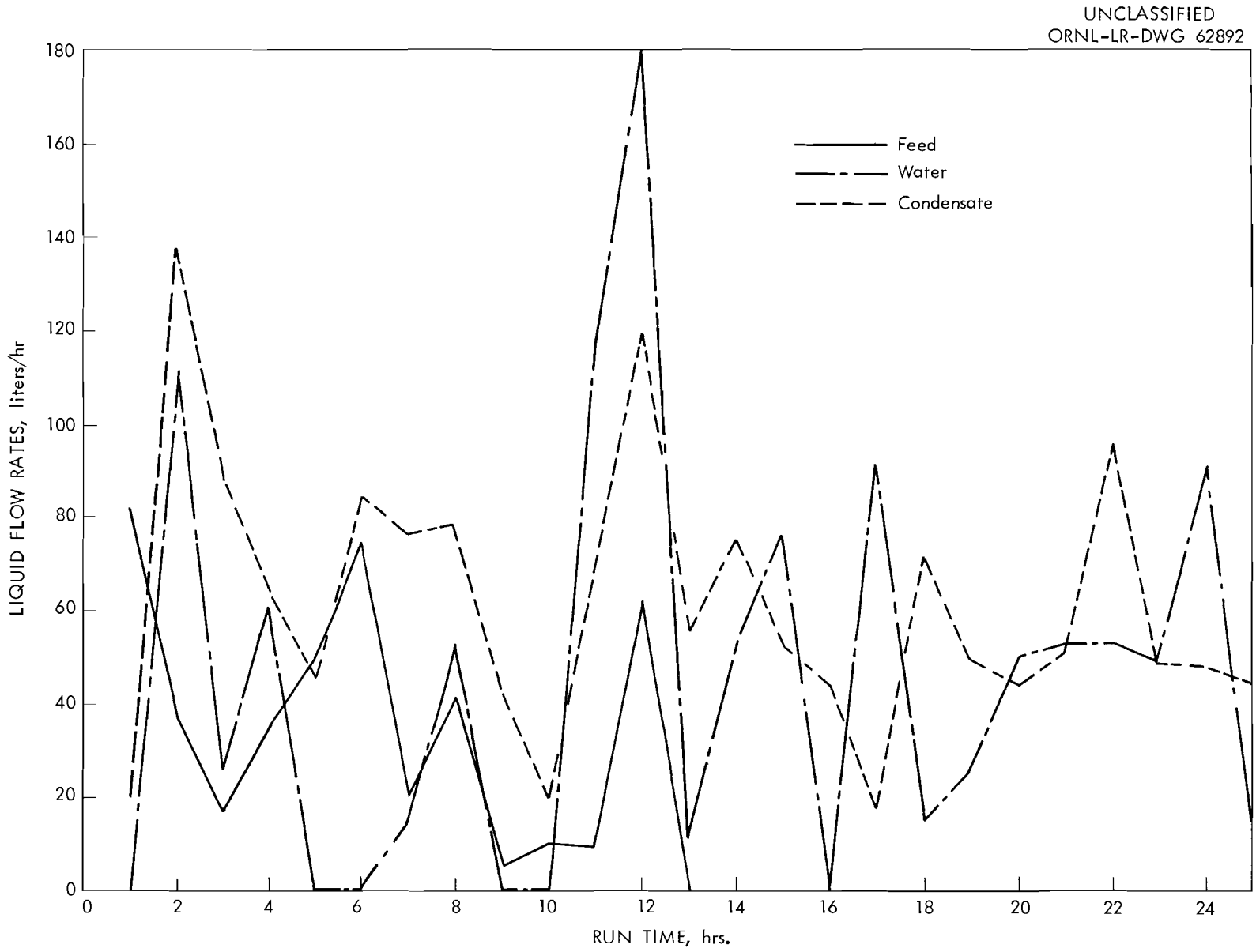

Fig. 8.1. System flow rates vs run time.

Table 8.3. R-38 Test Conditions and Results

Test Time	System Feed (TBP-25)	System Water Feed	Water to Feed Ratio	System Condensate	Evap Press	Mol NO_3 Input	Mol NO_3 Condensate	Evap Density	Evap Temp	Evap Al Conc	Evap Hg Conc	Evap Ru Conc	Evap H^+ Conc	Evap Steam Temp	Evap Steam Cond
hrs	ℓ	ℓ	ratio	ℓ	psig	g mol	g mol	g/cc	°C	g/ℓ	g/ℓ	g/ℓ	molar	°C	ℓ
1	82	0	0	20	-0.5	541	30	1.33	114	50.4	6.25	0.171	0.76	136	99
2	119	110	0.92	158	-0.5	785	85	1.37	111	56.7	6.88	0.234	3.25	126	198
3	136	136	1.00	246	-0.5	898	296	1.35	117	34.7	4.48	0.376	5.87	130	297
4	172	197	1.14	310	-0.5	1135	539	1.32	117	24.7	3.00	0.205	7.03	128	396
5	221	197	0.89	356	-0.75	1459	741	1.30	114	48.7	5.50	0.247	4.00	120	495
6	295	197	0.67	441	-0.75	1947	1063	1.32	118	54.7	6.13	0.205	3.56	129	594
7	315	212	0.67	517	-0.75	2079	1359	1.33	118	53.8	5.88	0.138	2.96	134	693
8	356	265	0.74	595	-0.75	2350	1608	1.35	112	48.6	6.63	0.142	4.27	122	792
9	361	265	0.73	637	-0.75	2383	1763	1.38	115	53.3	7.63	0.139	4.04	119	891
10	371	265	0.71	657	-0.75	2449	1853	1.38	117	58.9	8.75	0.154	1.70	121	990
11	380	382	1.01	730	-0.75	2508	1991	1.27	112	40.6	4.48	0.086	0.62	124	1089
12	442	617	1.40	849	-0.75	2917	2098	1.32	111	28.0	2.91	0.049	0.34	120	1188
13	442	628	1.42	904	-0.75	2917	2137	-	42	26.6	2.50	0.037	0.72	108	1287
14	442	681	1.54	979	-0.75	2917	2152	1.14	104	17.1	2.06	0.035	1.34	112	1386
15	442	757	1.71	1031	-0.75	2917	2157	1.13	104	14.0	1.75	0.021	1.70	116	1485
16		757	1.71	1075	-1.0		2161	1.15	103	11.0	1.55	0.024	1.98	114	1584
17		848	1.92	1092	-0.75		2164	1.13	103	7.91	1.15	0.014	2.11	115	1683
18		863	1.95	1163	-0.75		2178	1.12	42	6.02	1.05	0.010	2.22	113	1782
19		889	2.01	1212	-0.75		2183	1.12	104	4.67	0.70	0.010	2.24	114	1881
20		939	2.12	1256	-0.75		2196	1.12	102	4.76	1.08	0.013	3.28	115	1980
21		992	2.24	1307	-0.75		2237	1.10	107	5.01	3.35	0.020	5.83	112	2079
22		1045	2.36	1402	-0.75		2341	1.20	104	4.94	3.25	0.022	5.50	117	2178
23		1094	2.48	1450	-0.75		2393	1.25	110	5.45	3.63	0.022	5.25	115	2277
24		1185	2.68	1498	-0.75		2441	1.14	108.5	5.76	6.88	0.022	5.10	114	2376
25		1200	2.71	1542	-0.75		2476	1.14	108	5.94	10.1	0.021	4.90	113	2475
26		1264	2.86	1594	-0.75		2507	1.13	106.7	5.94	12.1	0.021	4.73	111	2574
27		1279	2.89	1638	-0.75		2529	1.12	105.7	6.12	12.9	0.026	4.63	111	2673
28		1329	3.01	1680	-0.75		2546	1.12	105.2	5.88	16.4	0.023	4.44	110	2772
29		1423	3.22	1721	-0.74		2558	1.12	104.8	5.94	17.8	0.025	4.45	110	2871
30		1457	3.30	1755	-0.75		2565	1.10	103.8	6.12	28.3	0.028	4.03	106	2970

Table 8.3. (Continued)

Test Time	Calciner Heat Input	Calciner Temp at Feed Point	Calciner Temp at Midsection Center	System Off-gas	Off-gas before Water Scrub						Off-gas after Water Scrub				
					N_2 Air	O_2	A_2	NO_2 + CO_2	NO_2	Air	N_2	O_2	A_2	N_2O	NO_2
					78.03	21.00	0.94	0.03	0						
hrs	KWH	°C	°C	cu ft	vol %	vol %	vol %	vol %	vol %	cu ft	vol %	vol %	vol %	vol %	vol %
1	6	120	75	010	78.0	20.9	0.9	0.4	-	10.0	77.8	20.9	0.9	0.2	-
2	55	120	120	052	78.2	20.9	0.9	< 0.1	-	42.0	77.7	21.0	0.9	-	-
3	104	135	135	095	77.8	21.1	0.9	0.2	-	42.9	78.0	21.0	0.9	-	-
4	150	145	145	122	75.7	24.1	0.9	0.1	-	26.2	77.2	22.1	0.9	0.1	-
5	199	145	145	159	77.6	21.9	0.9	-	-	36.8	77.8	21.8	0.9	-	-
6	245	145	145	171	67.7	29.8	0.8	0.3	1.0	10.4	66.1	31.4	0.8	0.5	-
7	282	145	145	201	65.5	31.1	0.8	0.4	1.7	25.2	67.1	31.6	0.8	0.5	-
8	321	130	130	245	73.0	24.5	0.9	0.2	1.8	41.2	74.5	23.9	0.9	1.1	-
9	340	135	135	285	74.0	23.5	0.9	0.1	2.6	38.0	74.0	24.3	0.9	0.5	-
10	363	135	135	311	70.0	28.3	0.8	0.3	1.0	23.3	72.0	27.4	0.9	0.3	-
11	380	125	125	362	77.4	21.5	0.9	0.4	-	50.6	74.2	24.6	0.9	0.5	0.2
12	394	130	130	309	76.9	21.5	0.9	0.1	-	52.3	75.7	22.7	0.9	0.4	-
13	406	130	130	359	73.3	24.7	0.9	0.3	0.3	47.0	74.1	24.8	0.9	0.3	-
14	422	130	130	406	74.1	24.1	0.9	0.1	1.2	44.7	74.2	24.3	0.9	0.3	-
15	436	130	130	438	76.3	22.0	0.8	0.5	0.1	31.3	77.5	20.9	0.9	-	-
16	448	130	125	590	78.1	21.0	0.9	-	-	152.0	74.2	24.4	0.9	0.4	0.2
17	462	130	125	620	77.4	21.1	0.9	0.1	0.3	29.8	74.8	23.8	0.9	0.4	0.1
18	479	135	125	671	74.5	24.3	0.9	0.2	0.2	48.7	73.8	24.7	0.9	0.2	-
19	495	130	125	728	74.1	24.7	0.9	0.2	0.6	54.2	74.2	24.1	0.9	0.4	0.1
20	507	130	125	769	77.0	20.9	0.9	-	-	40.5	71.4	26.9	0.9	0.5	0.1
21	518	145	135	819	73.1	25.7	0.9	0.1	0.9	46.9	71.8	26.7	0.9	0.6	-
22	536	180	140	860	71.9	26.2	0.9	0.2	1.0	37.8	72.3	26.9	0.9	0.4	-
23	543	275	140	914	71.1	27.0	0.9	0.2	1.0	49.2	71.2	27.4	0.9	0.4	-
24	559	405	150	964	67.3	30.3	0.8	0.2	0.9	43.2	68.6	29.9	0.8	0.4	-
25	571	610	150	1003	68.0	30.8	0.8	0.2	0.7	34.0	68.5	30.5	0.8	0.4	-
26	583	790	160	1038	69.5	28.9	0.8	0.1	0.4	31.2	69.5	28.8	0.8	0.3	-
27	593	820	185	1083	69.2	29.6	0.8	0.2	0.4	39.9	69.4	29.1	0.8	0.2	-
28	604	770	230	1135	70.9	27.6	0.8	0.2	0.2	47.3	71.0	27.8	0.8	0.2	-
29	614	770	315	1176	70.2	28.3	0.8	0.1	0.2	36.9	70.9	27.8	0.8	0.2	-
30	621	800	800	1221	74.1	25.0	0.9	0.1	0.1	42.8	74.3	25.1	0.9	0.2	-
				1262						1151.8					

Table 8.4. Test R-38 Operation Log

Run Time		
0	8:00	Start Wheelco 800°C - Evaporator full cold - pot empty cold
0.5	8:35	Start to fill pot - Evaporator 114°C - pot furnace on
1.0	9:00	Calciner pot full
2.5	10:30	Calciner level plugged - water added 50 cc/min
5.0	13:00	Evaporator pressure set point moved -0.5 psig to -0.75 psig
11.0	19:00	Low rate of feed to the calciner pot - evaporator standby
13.0	21:00	System foam over to condenser
24.0	8:00	Wheelco to 900°C
31.0	14:00	Calciner heat off and evaporator shut down

Table 8.5. Control Setting for Test R-38

	Control Variable	Control Range 0 - 100%	Prop. Band %	Reset min	Set Point Scale %
Evaporator	Liquid level	7.4-35.0 liter	250	5	50
Evaporator	Density	1.0-1.5 g/cc	200	10	70
Evaporator	Temperature	101-128 °C	100	5	65
Evaporator	Pressure	-5 to +5 psig	10	0.3	42
Calciner	Liquid level	44-52 liter	100	10	50

Table 8.6. Operational Limits for Test R-38

	Limit A	Limit B	Set Point	Limit C	Limit D	Operational* Readings Min	Max
Evaporator Liquid Level							
scale %	90	65	50	35	25	35	60
liters	33	26	22	18	15	18	24
Evaporator Density							
scale %	80	70	65***	50	40	20	78
g/cc	1.40	1.35	1.32	1.25	1.20	1.10	1.39
Evaporator Temperature							
scale %	90	75	65	30	0	67	2
°C	122	120	117	110	103	118	102
Evaporator Pressure							
scale %	47	45	42	40	38	45	35
psig	-0.25	-0.50	-0.75	-1.0	-1.25	-0.5	-1.5
Calciner Liquid Level							
scale %	30	40	50	60	70	20	80**
liters	58	59	60	61	62	57	63

* Recorded hourly readings
** Was zero before and after filling period
*** Al ≅ 45 g/liter

UNCLASSIFIED
ORNL-LR-DWG 62893

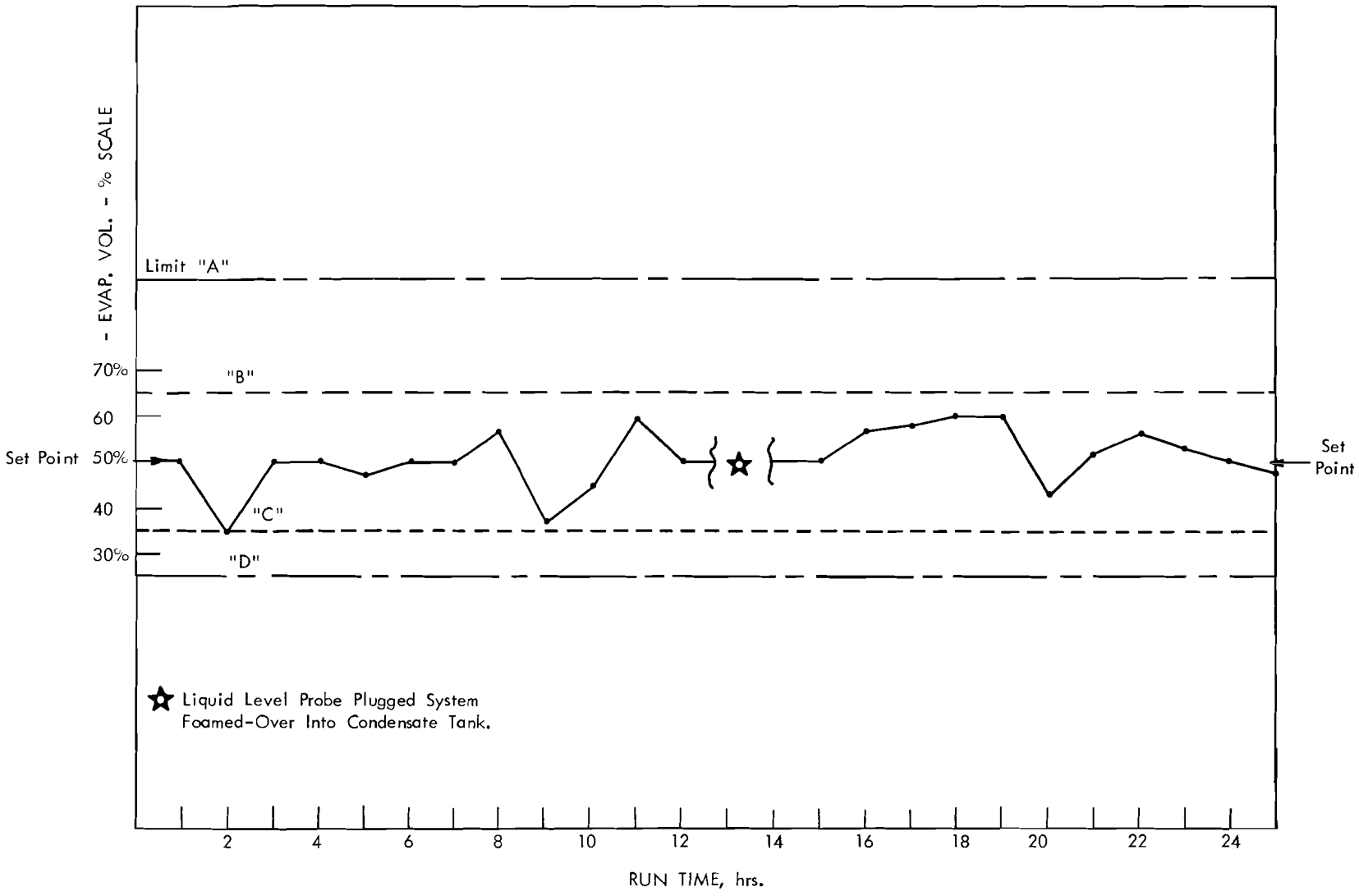

Fig. 8.2. Evaporator liquid level vs time.

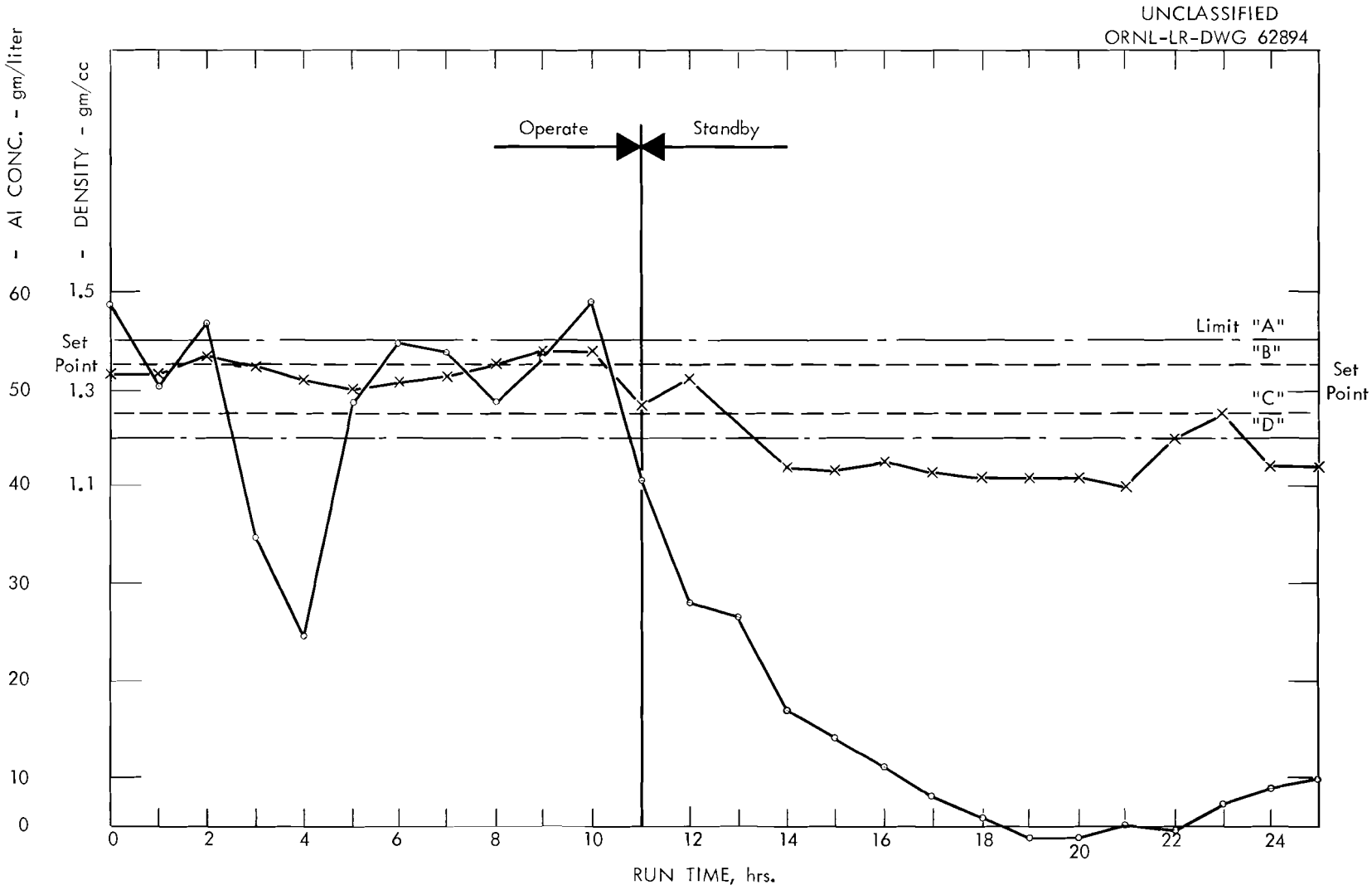

Fig. 8.3. R-38 evaporator density and Al concentration vs run time.

very closely, Figure 8.4. The high acid level of the 4th hour did not cause any extra Ru volatility. The Ru in the condensate was below 0.005 g/liter for the entire test. The maximum evaporator Ru concentration was 0.25 g/liter.

8.3 Calciner Pot Corrosion

The calciner pot used in test R-38 showed no signs of corrosion on the inside. The outside of the pot showed no signs of corrosion or oxidation scaling. A nitrogen purge of 10 cu ft/hr was used between the calciner pot and furnace liner.

8.4 Calcined Solid

The calcined solid had a bulk density of 0.56 g/cc (Tables 8.2 and 8.7). The solid was light gray in color and very crumbly. There was a hole down the center of the pot indicating radial growth of solids. Only 4% of the mercury fed to the system remained with the calcined solids. However, 43% of the ruthenium added as cold ruthenium remained with the calcined solid. The off-gas line contained a solid film which was 90% mercury and 1% Ru. The mercury and ruthenium system balances were 57% and 42%. The unaccounted for material probably plated on the system's metal surfaces.

8.5 Off-Gases

The off-gases were sampled before and after the water jet scrubber. The gases were analyzed for O_2, N_2, A, NO-CO_2, and NO_2, Table 8.3. After sampling,the gas volume is determined by a wet test meter. The total volume of gas for the test was 1260 cu ft, of which 1152 cu ft was leakage and instrument purge (~400 cu ft purge). Of the 108 cu ft of non-condensables other than air, 74 cu ft was excess oxygen, and the remaining 34 cu ft was NO_2.

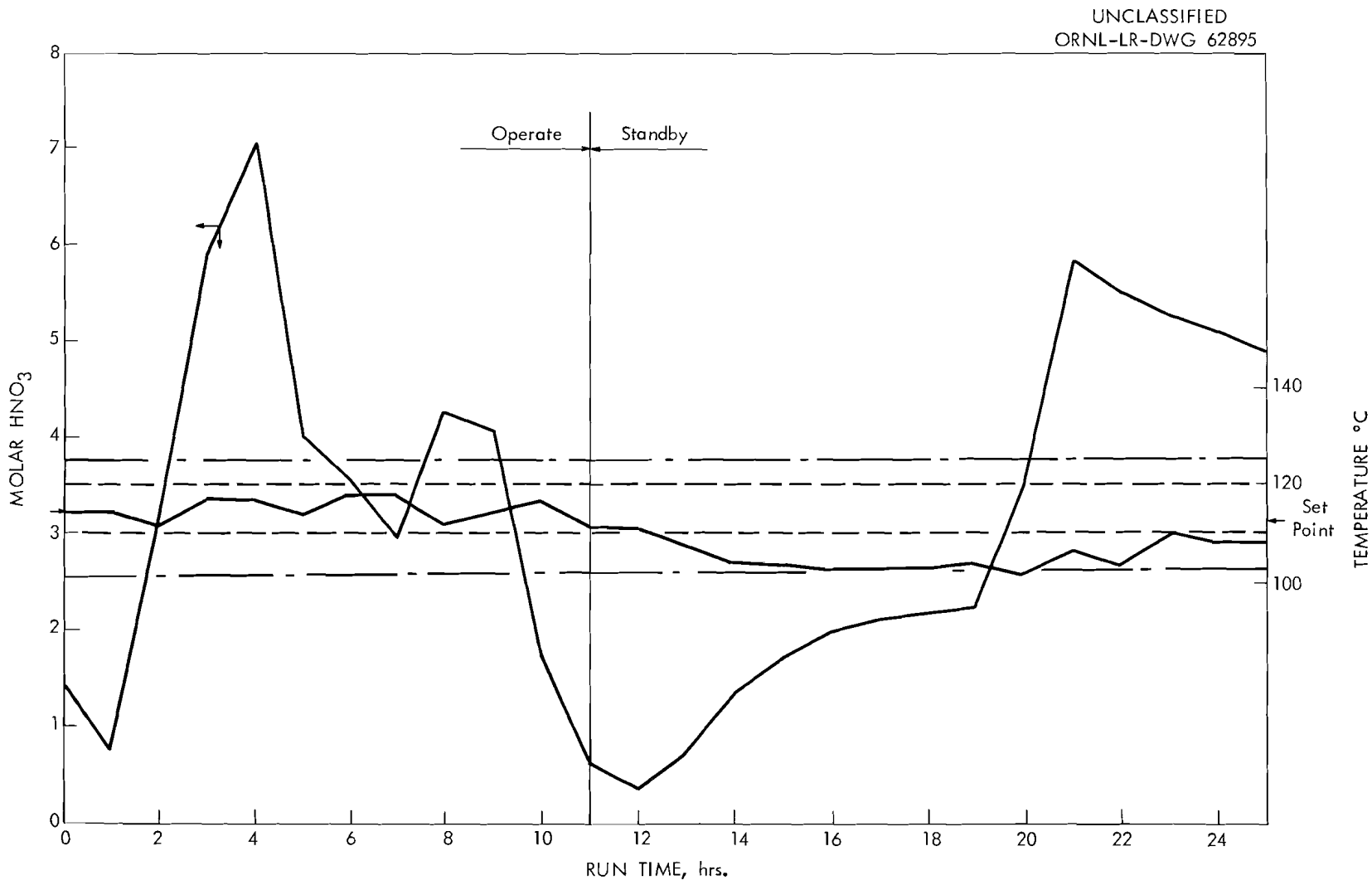

Fig. 8.4. R-38 evaporator temperature and acid concentration vs run time.

Table 8.7. R-38 Solid Analysis

		Fe wt %	Al wt %	Hg wt %	NO_3 wt %	Ru mg/g
Top	70 in.	0.48	42.5	0.84	1.7	1.2
	50 in.	0.35	44.0	0.1	0.2	0.5
	30 in.	0.38	46.0	0.1	0.3	0.5
Bottom	6 in.	0.39	46.0	0.1	0.1	0.7

DISTRIBUTION

1. E. L. Anderson (AEC Washington)
2. F. P. Baranowski (AEC Washington)
3. W. G. Belter (AEC Washington)
4. S. Bernstein (Paducah)
5. R. E. Blanco
6. J. O. Blomeke
7-10. J. C. Bresee
11. R. E. Brooksbank
12. K. B. Brown
13. F. R. Bruce
14. J. A. Buckham (ICPP)
15. L. P. Bupp (HAPO)
16. W. D. Burch
17. W. H. Carr
18. G. I. Cathers
19. J. T. Christy (HOO)
20. W. E. Clark
21. V. R. Cooper (HAPO)
22. K. E. Cowser
23. F. E. Croxton (Goodyear Atomic)
24. F. L. Culler, Jr.
25. W. Davis, Jr.
26. O. C. Dean
27. D. E. Ferguson
28. L. M. Ferris
29. R. J. Flanary
30. E. R. Gilliland (MIT)
31. H. E. Goeller
32. M. J. Googin (Y-12)
33. H. B. Graham
34. A. T. Gresky
35. P. A. Haas
36. M. J. Harmon (HAPO)
37. F. E. Harrington
38. L. P. Hatch (BNL)
39. O. F. Hill (HAPO)
40. J. M. Holmes
41. R. W. Horton
42. A. R. Irvine
43. G. Jasny (Y-12)
44. H. F. Johnson
45. W. H. Jordan
46. S. H. Jury
47. K. K. Kennedy (IDO)
48. B. B. Klima
49. E. Lamb
50. D. M. Lang
51. S. Lawroski (ANL)
52. R. E. Leuze
53. W. H. Lewis
54. J. A. Lieberman (AEC Washington)
55. R. B. Lindauer
56. A. P. Litman
57. J. T. Long
58. B. Manowitz (BNL)
59. J. L. Matherne
60. J. A. McBride (ICPP)
61. J. P. McBride
62. W. T. McDuffee
63. R. A. McGuire (ICPP)
64. R. A. McNees
65. R. P. Milford
66. J. W. Morris (SRP)
67. E. L. Nicholson
68. J. R. Parrott
69. F. S. Patton, Jr. (Y-12)
70. H. Pearlman (AI)
71. R. H. Rainey
72. J. T. Roberts
73. K. L. Rohde (ICPP)
74. C. A. Rohrmann (HAPO)
75. A. D. Ryon
76. W. F. Schaffer, Jr.
77-79. E. M. Shank
80. M. J. Skinner
81. C. M. Slansky (ICPP)
82. S. H. Smiley (ORGDP)
83. J. I. Stevens (ICPP)
84. C. E. Stevenson (ANL, Idaho)
85. K. G. Steyer (General Atomics)
86. E. G. Struxness
87. J. C. Suddath
88. J. A. Swartout
89. F. M. Tench (Y-12)
90. V. R. Thayer (duPont, Wilmington, Del.
91. W. E. Unger
92. J. Vanderryn (AEC ORO)
93. F. M. Watzel (ICPP)
94. C. D. Watson
95-124. M. E. Whatley
125. G. C. Williams
126. R. H. Winget
127. C. E. Winters
128. R. G. Wymer
129-130. Central Research Library
131-134. Laboratory Records
135. Laboratory Records (RC)
136. Document Reference Section
137. Research and Development Division
138-152. DTIE